TIME RESOLVED LUMINESCENCE MEASUREMENTS ON POLYDIACETYLENES, AN ORDERED AND ISOLATED ONE DIMENSIONAL MODEL SYSTEM

THÈSE N^{O} 3436 (2006)

PRÉSENTÉE À LA FACULTÉ SCIENCES DE BASE

Institut de photonique et d'électronique quantiques

SECTION DE PHYSIQUE

ÉCOLE POLYTECHNIQUE FÉDÉRALE DE LAUSANNE

POUR L'OBTENTION DU GRADE DE DOCTEUR ÈS SCIENCES

PAR

Christian BLUMER

ingénieur physicien diplômé EPF
de nationalité suisse et originaire de Glaris (GL) et de Freienstein-Teufen (ZH)

acceptée sur proposition du jury:

Dr J.-D. Ganière, directeur de thèse
Prof. C. Félix, rapporteur
Dr R. Grousson, rapporteur
Dr P. Renucci, rapporteur

Lausanne, EPFL
2006

Abstract

In this work time resolved luminescence measurements on the red phase of 3BCMU are presented. These polydiacetylenes form an ordered and isolated one dimensional model system. This work is divided in two parts. First we present an excitation spectrum in chapter 4. In the second part, radiative lifetimes are examined at temperatures down to 2 K (chapter 5).

We present studies on excitation spectra on the red phase of 3BCMU up to an excitation energy of 850 meV above the zero phonon excitonic line. The vibronic modes of the double and triple bond of the carbon of the backbone and their combinations are identified. Compared to luminescence spectra a small anharmonicity is found. Also a relatively small Huang-Rhys factor is obtained, a parameter describing the decrease in intensity of the successive multiple of a vibronic mode. This is a result expected for such a complex system as a polymer. Furthermore, any signature of the band edge is absent in the spectrum. This result is interesting, as the theory predicts a suppression of the van Hove singularity at the band edge. Experimental results on other one-dimensional systems on this subject are rare.

The radiative lifetime is a parameter which is dependent on the dimensionality of the structure. In the special case of one-dimensional systems it is predicted to be proportional to the square root of the temperature. Measurements of other one-dimensional systems show that the law is broken at relatively high temperatures (around 30 K) because of fluctuation of the confinement potential, which leads to localisation. For our sample, the radiative lifetime follows the mentioned law to a temperature down to 2 K. However, we show that in samples of less quality, mainly due to ageing, the law is not valid anymore. This ageing of the sample is caused by a higher polymerisation rate and defect in the crystalline structure.

Version abrégée

Dans ce travail, nous présentons des mesures de photoluminescence résolue en temps sur la phase rouge du 3BCMU. Ce poly-diacétylène constitue un système modèle pour un système isolé et unidimennsionel. Ce manuscript est divisé en deux parties. La première traitant des mesures d'excitation présentées dans le chapitre 4, et la deuxième présentant des travaux sur les temps radiatifs à des températures aussi basses que 2 K.

Nous avons mesuré des spectres d'excitation jusqu'à 850 meV au dessus de l'énergie de l'exciton. Les modes vibroniques, ainsi que leurs combinaisons, des liaisons doubles et triples du carbon situées dans la chaine du polymère ont étés identifiés. Nous avons trouvé une petite anharmonicité en comparant ces valeurs avec celles des spectres de luminescence. De plus, un facteur de Huang-Rhys relativement petit a été déterminé, caracteristique pour des systèmes complexes comme un polymère. Ce facteur décrit l'attenuation des intensités des modes vibroniques et leurs multiples entre eux. Ensuite, nous n'avons trouvé aucune trace du bord de bande des porteurs libres. Ceci est bien prédit par la théorie, neanmois les résultats expérimentaux sont rares sur ce sujet. Les théories prédisent une atténuation de la singularité de van Hove au bas de la bande.

Le temps radiatif est un paramètre qui dépend de la dimension de la structure qui confine les espèces recombinantes. En particulier pour un système à une dimension, le temps radiatif est proportionnel à la racine de le la température. Des travaux sur d'autres systèmes à une dimension montrent que cette loi n'est suivie que pour des températures supérieures à 30 K. Des fluctuations du potentiel de confinement localisent les porteurs. Les mesures sur notre échantillon montrent que la loi est confirmée pour des températures supérieures à 2 K. D'autre part nous avons remarqué que ceci cesse d'être vrai pour des échantillons agés. Une augmentation du taux de polymerisation et des défauts de structure du cristal sont à l'origine de cette déviation.

Zusammenfassung

Die vorliegende Arbeit handelt über zeitaufgelöste Lumineszenzmessungen von 3BMU, einem Polydiacethylen, das ein Modellbeispiel für isolierte, eindimensionale Systeme ist. Der Text ist in zwei Teile gegliedert. Der erste handelt über Anregunsmessungen und ist im Kapitel 4 zu finden. Im zweiten Teil präsentieren wir Messungen der radiativen Lebenszeit für Temperaturen bis zu 2 K (Kapitel 5).

Die Anregunsmessungen der roten Phase des 3BCMU erstrecken sich bis zu einer Energie von 850 meV über dem Grundzustand des Exzitons. Die Vibrationsmoden der Doppel- und Dreifachbindungen zwischen den Kohlenstoffatomen der Polynomkette und deren Kombinationen konnten identifiziert werden. Deren spektrale Positionen, verglichen mit Fluoreszenzspektren, lassen auf eine kleine Anharmonizität schliessen. Des Weiteren wurde ein kleiner Huang-Rhys Faktor ermittelt, wie er bei komplexen Systemen wie beispielsweise Polymeren üblich ist. Als weiteres Resultat ist hervorzuheben, dass wir keine Hinweise auf den spektralen Teil der freien Ladungsträger gefunden haben. Dies ist insofern interessant, als dies von Theorien vorhergesagt wird, Messungen von eindimensionalen Systemen aber selten sind.

Die radiative Lebenszeit ist abhängig von der Dimension der Struktur. Im Speziellen für eindimensionale Systeme ist sie proportional zur Quadratwurzel der Temperatur. Andere eindimensionale Systeme folgen diesem Gesetz nur bis zu einer Temperatur von rund 30 K. Ab dieser Region werden die Träger durch Fluktuationen des Potentials lokalisiert. In userem Fall konnten wir das Gesetz bis zu einer Temperatur von 2 K überprüfen. Dennoch ist die Eigenschaft sehr sensibel auf Störungen. Ältere Proben, deren Konzentration an Polymeren höher ist oder wo Fehler in der Kristallstrucktur zu erwarten sind, weichen vom oben genannten Gesetz ab.

Acknowledgements

I would like to thank my thesis director Dr. Jean-Daniel Ganière for his help and guidance during my project. I appreciated his availability and the discussions we shared about the encountered problems. I could always count on him to realign the laser system the next day, when it stopped to work in the worst moments.

I am grateful to Prof. Benoît Deveaud-Plédran who accepted me in his group and thus gave me the opportunity to work on this project.

A very special thank to Prof. Michel Schott with whom I enjoyed many discussions about polydiatylenes and physics in general. His support was an important reason for the success of my project. Without his guidance and profound knowledge my thesis would have been impossible in this form.

I am grateful to the "Groupe du Solide" at the Université 6 & 7 in Paris, where I could realise the absorption measurements of the T vibronic line. In particular, I want to mention Mrs. J. Berréhar who has grown the samples of 3BCMU.

To work in the "Laboratoire d'Optoélectronique Quantique" was a pleasure. Besides discussing different subjects related to physics, we shared a lot of activities in our free time together. I will remember the good spirit I experienced with my altering office colleagues, Michele, Sämi, Ferran, Pablo, Daniel, Pierre and Stéphane.

I want to thank the Swiss Academy of Engineering Sciences (SATW) which financed the several respective travels from and to Paris with the support program "Germaine de Staël". This work was also supported by the Swiss National Science Foundation (grant #200020-10016).

Finally, I wish to thank my parents for their continuous support and Yvonne for her understanding and patience, especially during the last months of my thesis.

Contents

1 Introduction

Organic semiconductors were for a long time only available in massive disordered form, where the chains had an important interaction. In the mid 90s, 3BCMU a diacetylene was produced, where the residual polymers in the monomer crystal have interesting characteristics. The monomer crystal is of good quality, such that the polymers are obtained in an ordered form. The residual polymer concentration in a freshly grown crystal is low in a way that the chains are isolated one from each other. Polydiacetylene exist in two different phases. For the 3BCMU they coexist and the blue phase, named this way because its absorption is of lower energy than that for the second one, the red phase, is the dominant one. Because of the comparably high quantum yield, luminescence measurements are possible. As the order of the lifetimes is around 100 ps, time resolved measurements with a streak camera can be performed.

The radiative lifetime depends on the dimensionality of the structure and for a one-dimensional system it is proportional to the square root of the temperature. Therefore the radiative lifetime is a parameter sensible to the fluctuations of the confinement potential. By the nature itself of the confinement of the carriers, the confinement potential has much less fluctuations than found in other one-dimensional systems. In the last years, a large number of papers were published on the characterisation and analysis of potential fluctuations for one-dimensional structures.

It was shown that the red phase of 3BCMU follows this law for temperatures from 10 K to 100 K. At higher temperatures the intensity of the signal becomes to weak because of a non radiative channel, which starts to dominate the recombination.

One aspect of this work is to investigate at which temperature the law will be broken. For temperatures below about 0.8 K, the theory used to derive the law becomes inconsistent. However, localisation of the excitons could break the law at a higher temperature. This was found to be the case for example in V-shape quantum wires at temperatures below 30 K. From a experimental point of view, the extension to lower temperatures than 10 K, opens some challenges. For our measurements at temperatures between 2 and 4 K, an helium bath cryostat was used. In controlling the sample temperature by a helium gas flow, its temperature range can be extended to higher temperatures. As the sample is expected to have inhomogeneous luminescence characteristics, the spatial stability of the setup becomes crucial.

We were able to show that the square root law is still valuable at 2 K. However, this law seems to be highly sensitive on the quality of the chains. We noticed that older samples had a radiative lifetime, which became con-

stant. We explain this by a higher polymer concentration and defects in the monomer crystal.

The measurements at low temperatures are presented in chapter 5. A second chapter (4) presents the analysis of excitation measurements. In the special case of the red phase of the 3CMU, these measurements are interesting, because an absorption spectrum can not be obtained. As the concentration of the blue phase is 4 orders of magnitude higher than the red one, the total absorption spectrum is essentially a spectrum of the blue phase. In the absence of additional recombination channels situated at higher energies than the exciton recombination energy, the absorption and excitation spectra are similar.

In one-dimensional systems the density of states present a singularity at the band edge because it goes as $1/\sqrt{E}$ (van Hove singularity). When including Coulomb interaction between the electron and holes, the exciton lines are introduced and the singularity disappears. In our excitation measurements there is no signature of the band edge, neither of the continuous states. Taking the blue phase as reference, we would expect a binding energy of around 0.5 eV. This value was obtained with electroabsorption measurements, which are not possible on the red phase. The binding energy is a parameter which depends on the lateral confinement and the electronic correlation.

When exciting with a energy of 2.540±4 eV, an additional peak only 8.5 meV lower in energy than the zero phonon line appears. With the data present, we are not able to give an explanation for this peak. Primarily excitation measurements with a higher excitation resolution than the 10 to 20 meV we had in our setup are needed.

2 Material and Samples

We present the basic structural and optical properties of diacetylenes. In the second chapter these properties are detailed on the polydiacetylenes this work was done with (3BCMU) to give a surrounding knowledge for the measurements presented in the chapters 4 and 5.

2.1 Chemical Structure and Sample Growth

Polydiacetylenes are conjugated polymers obtained by solid state polymerisation of the diacetylene monomer by the following formula:

$$n\ R-C\equiv C-C\equiv C-R' \rightarrow (=CR-C\equiv C-CR'=)_n$$

R and R' are lateral groups, which are identical and equal to $-(CH_2)_3-OCONHCH_2COOC_9H$ for 3BCMU, the (poly)diacetylenes studied in this work. For the chemical structure of the polymer see figure 1. Polydiacetylenes are found to exist in two different structures with the same chemical composition. Depending on their colour appearance in transmission, they are labelled the blue or the red structure. The blue structure absorbs at a wavelength around 630 nm and the red around 540 nm. A more precise criterion to distinguish between the two phases are the ground state vibrational energies. As example, the double bond stretch mode D has an energy of 179.8±1.2 meV for the blue phase and 188.5±1.2 meV for the red phase. Some polydiacetylenes show a phase transition of the first order from the blue to the red structure. Other exist only in one of the two structures. 3CBMU is up to date the only one known polydiacetylene, where the two phases coexist. However there exist some assumptions about the differences in the two structures. A model has been proposed, which explains the differences by an undulation of the backbone. Instead of being confined in a plane, as it is the case for the blue structure, the chain of the red structure would fit in a planar surface folded every unit length of the polymer backbone, having thus a repetition rate twice as long as the one for the blue phase (cf. figure 2). Diffraction measurements proved that the carbon backbone of the blue structure lays in a plane. These measurements are not possible for the red structure, because there does not exist a polydiacetylene of the red structure in a crystal of sufficient quality. However RMN measurements show a repetition length of the backbone which is doubled for the red structure compared to the blue[Tan89]. The undulation could explain the absorption at higher energies of the red structure. Approximate calculations show that the energy of the absorption rises for bigger angles in the undulation and an angle of $\theta \sim 25°$ is found [Lec00].

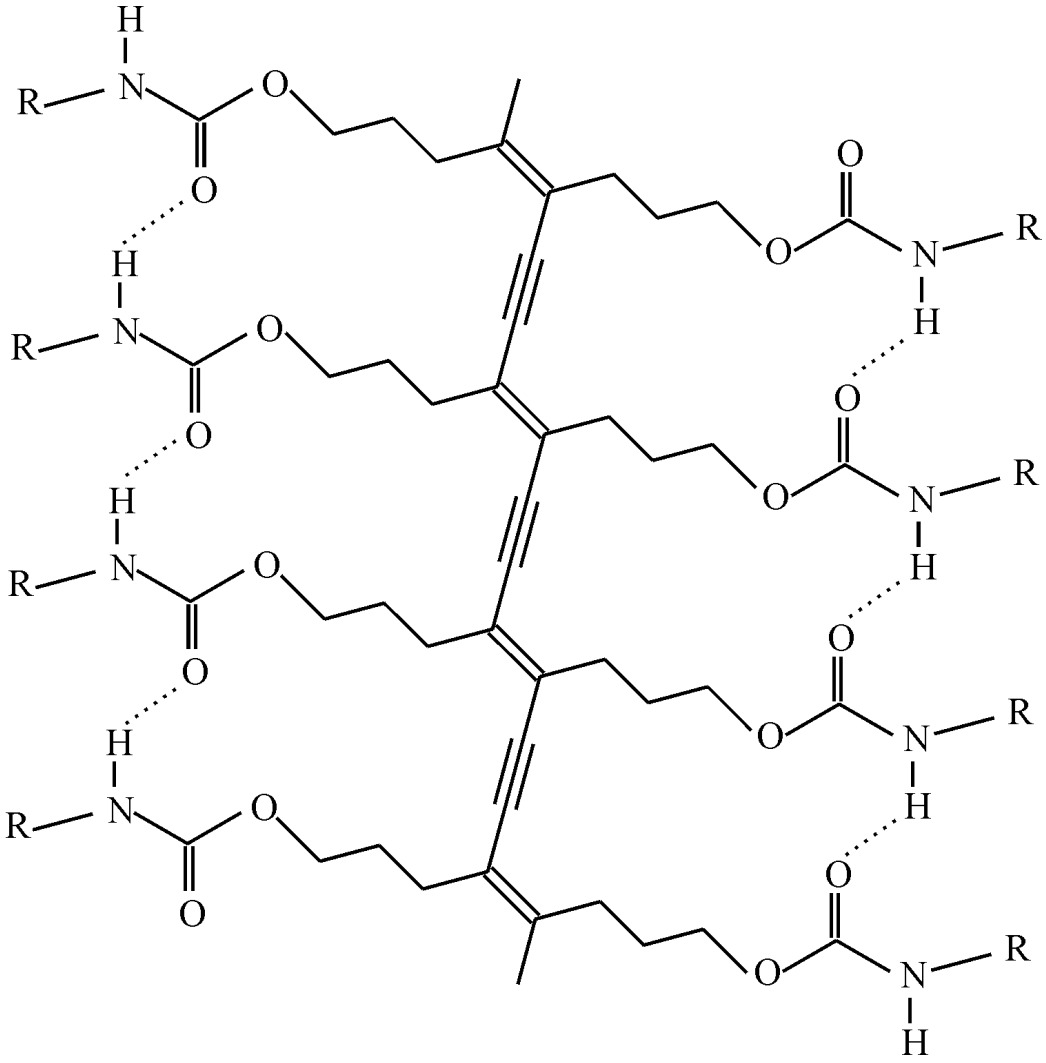

Figure 1: Chemical structure of a polydiacetylene. The thick dotted line indicates the backbone of the polymer. Note the two lines of H-bonds running parallel to the polymer chain in the plane a×b.

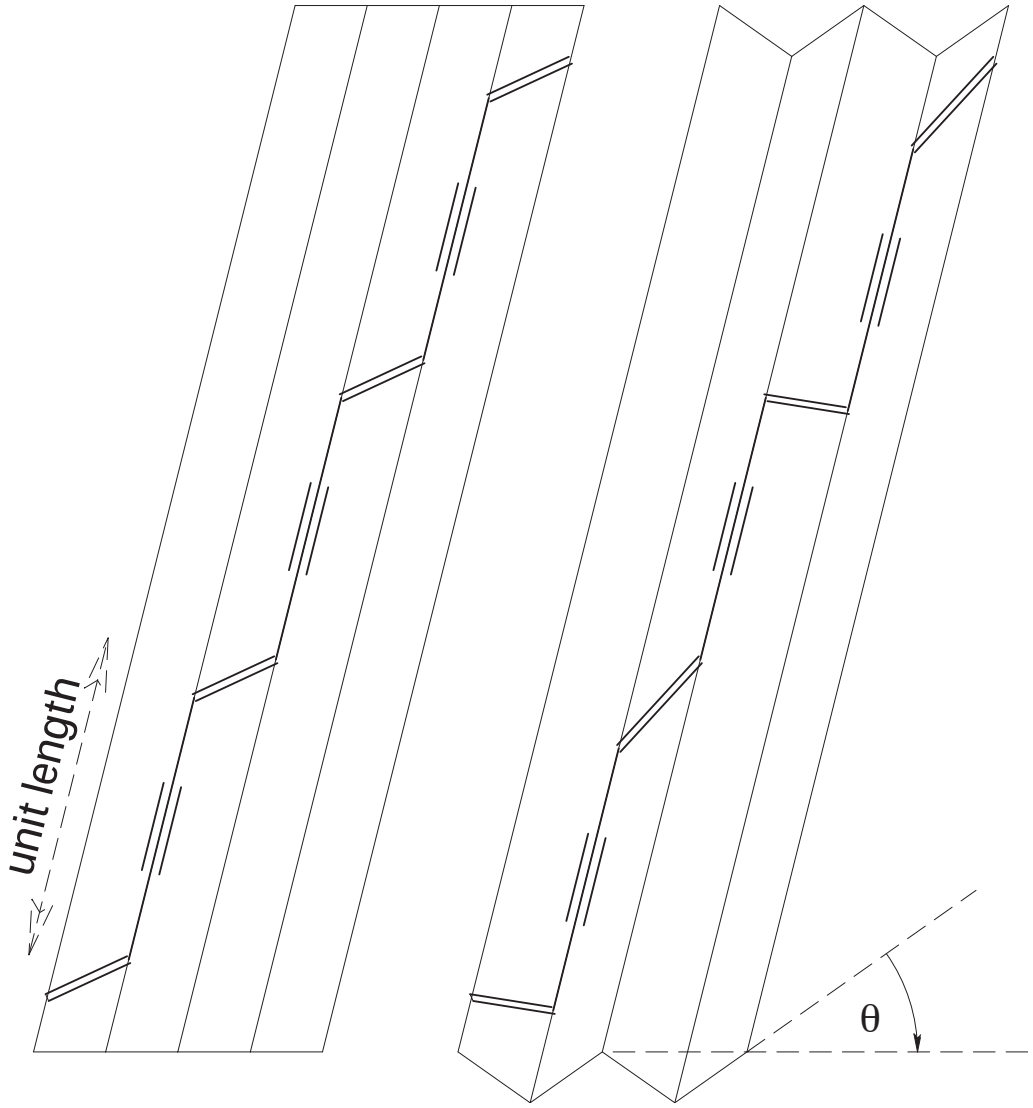

Figure 2: The chain of the red structure is supposed to undulate at an angle θ, whereas the blue structure is planar. On the left is the planar blue structure and on the right the undulated red structure.

Only a sub-group of the diacetylenes form crystals in the solid state. This depends on the lateral group. The monomer crystal has a mono-clinic structure. 3BCMU has the the following lattice parameters at 93 K, which do not differ largely from other diacetylene crystals:
a = 58.607 Å, b = 4.858 Å, c = 8.943 Å, $\beta = 97.59°$.
A unit cell is formed of four molecules[Sch].

The crystals are grown in a solution of purified 3BCMU oligomers and acetone at 4 °K. The process has to be done in the dark to avoid polymerisation iniciated by ambient light. Further details of the production process can be found in [Spa95, chapter II.2]. At the end of the growth, the sample have typically a quadrangular surface of several ten of mm^2 and a thickness between 50 and 300 μm. The as grown monomer crystals have a residual polymer concentration of $x_p = 10^{-4}$ in weight. The polymer concentration does not change with temperature but can be augmented by γ irradiation to the desired level[Spa96]. The polymer chains are oriented parallel to the edge of one side of the larger surface of the sample. The exact orientation can be detected with a polariser oriented in the same direction as the chains because of a large dichroism of the absorption and emission of the polymers.

As mentioned above, the polymer concentration can be augmented to a desired value. 3BCMU can also be prepared either in a solution or as thin films. Therefore the monomer crystal has to be dissolved by an usual organic solvant, as chloroforme for example to obtain a solution. In irradiating the cristal with electrons, thin films with more ordered polymers can be produced. The energy and therefore the penetration distance of the electrons define the width of the film situated on top of the monomer crystal. This film can be detached of the crystal by dissolving the monomers.

Of all the different forms in which polydiacetylenes can be produced, the diluted polymers in the monomer crystal are of special interest. They are a model system for isolated and oriented chains, necessary for the measurements presented in this work. The samples were grown at the INSP of the Université Paris 7.

3BCMU crystal cannot be polymerised totally but all known polydiacetylene crystals have a repeat distance along the chain of 4.89 ± 0.02 Å. Therefore the lattice mismatch is smaller than 0.5 % and minimal stress is expected along the chains. During the polymerisation the lateral groups are known to change their positions to compensate a slight rearrangement of the backbone of the polymers. Therefore, it is possible that a more important stress exists in the other directions.

The length of the polymers has been measured by light scattering and is 10 - 15 μm[Bared]. Recent spatially resolved micro-photoluminescence measurements show that the length of a polymer chain can be as large as

20μm[Dub04]. These experiments indicate also that the 3BCMU polymer is either in the red or blue structure and that the chain is not separated in segments of the two different structures.

The mean distance between two polymers is about 100 nm in a crystal with a polymerisation rate of 10^{-4} [Lec00]. The characteristics listed above show that polydiacetylenes are a model for one dimensional systems which are ordered because of the polymerisation in the crystal matrix.

2.2 Optical and Electronic Properties of 3BCMU

2.2.1 Blue Phase of 3BCMU

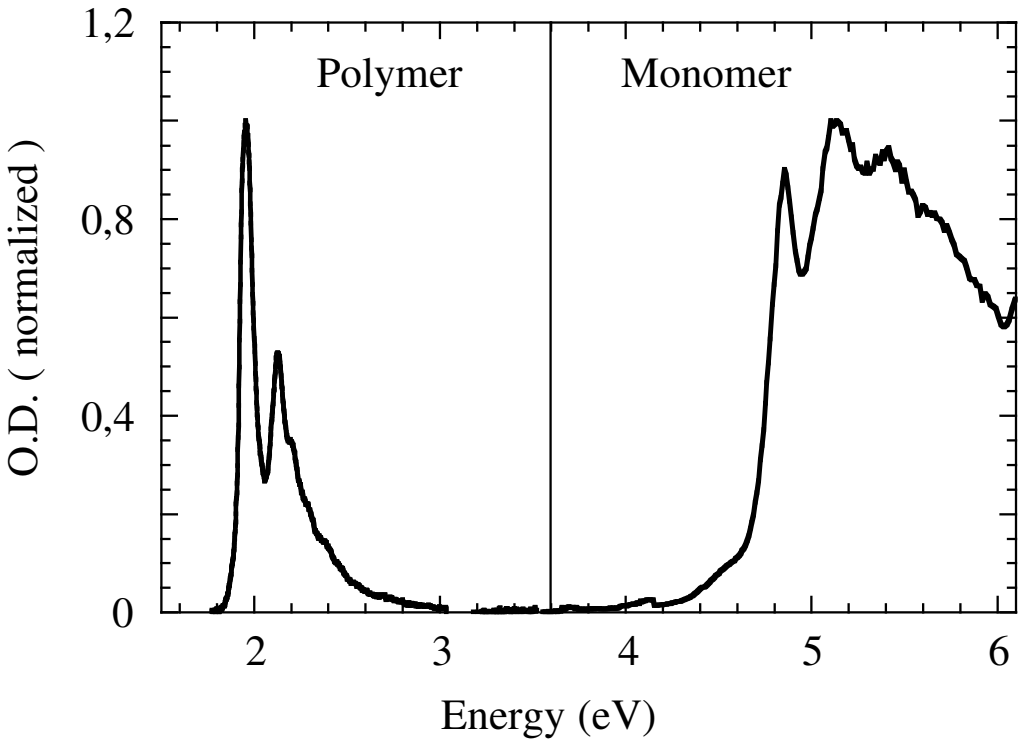

Figure 3: Absorption spectrum at room temperature of a crystal of 3BCMU polymerised to $x_p \sim 0.1\%$. The absorption of the monomer and the polymer are well separated by around 2.5 eV. 10^4 cm$^{-1} \approx 1.24$ eV

The optical absorption spectra of the monomer and the polymer are well separated by 2.5 eV for the 3BCMU (cf. figure 3). In figure 4 an absorption spectrum of the polymer at 10 K is shown.

The spectrum on figure 4 shows an absorption with an excitonic peak at 1.9 eV and several peaks of vibrational modes at higher energies. The

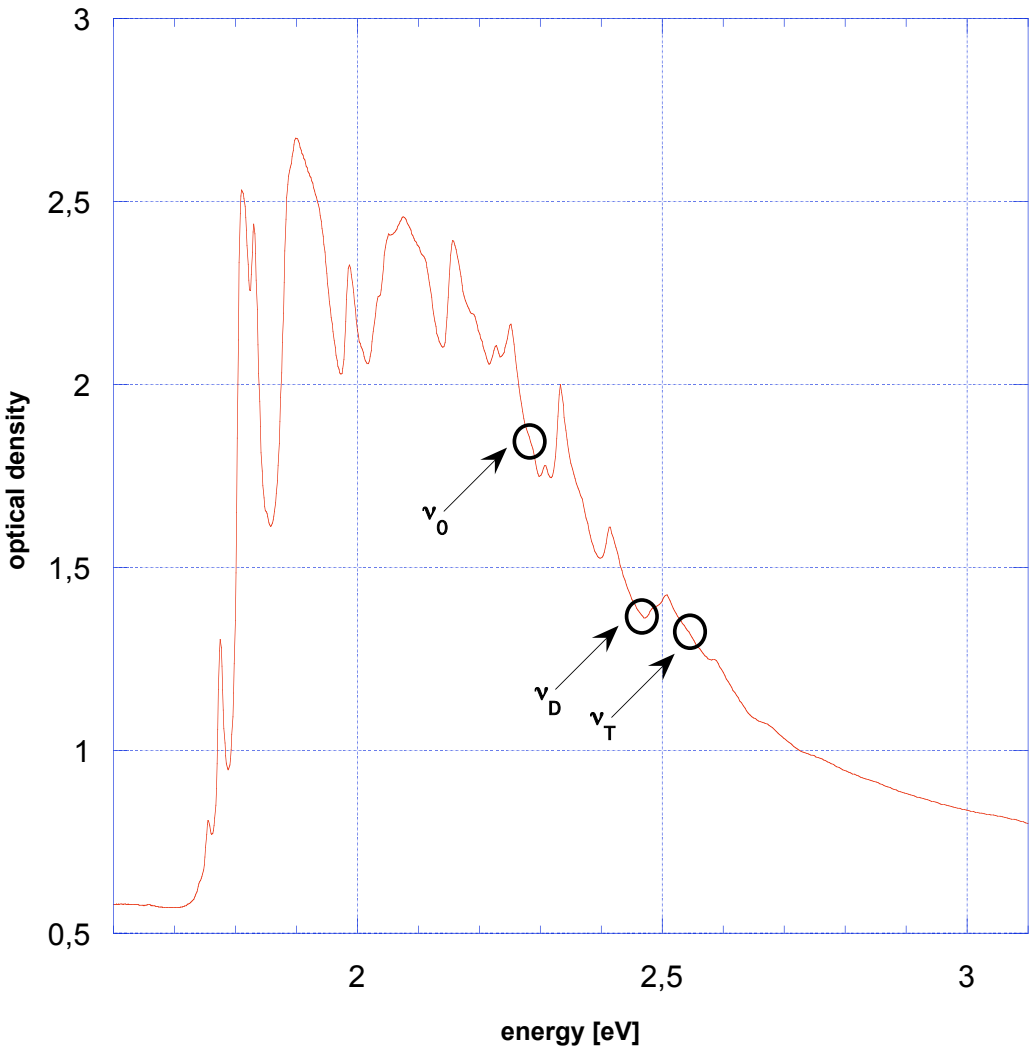

Figure 4: Absorption spectrum of a diluted poly-3BCMU crystal at 10 K. The three most intense absorption lines of the red phase are highlighted by circles. They correspond to the zero phonon line (ν_0), the D and T phonon line (ν_D, ν_T).

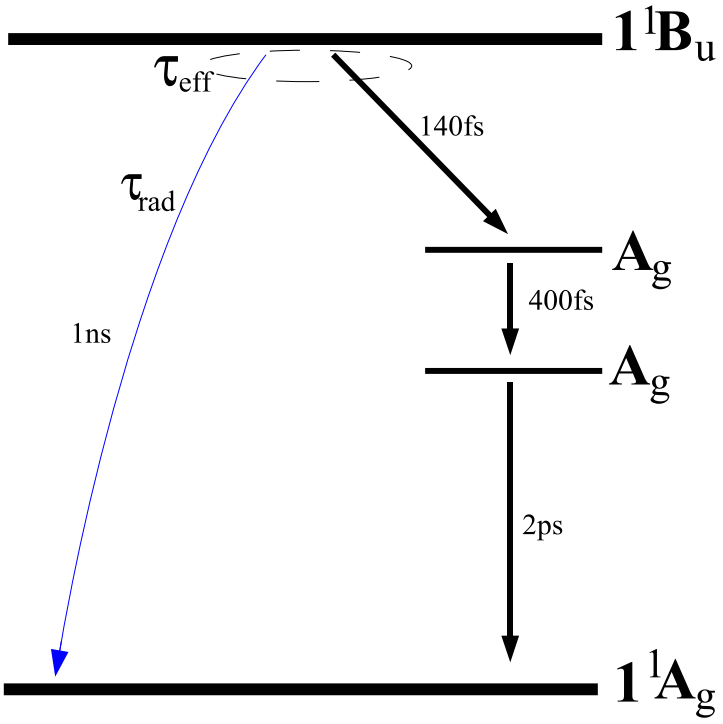

Figure 5: Scheme of the non radiative channels which dominate completely the recombination of the blue phase.

peaks below 1.9 eV are shown to be chains having slightly different ground state geometries[Hor97]. This absorption corresponds to the blue structure. The fluorescence is very weak, with a quantum yield around 1-2·10^{-4}[Spa94]. Indeed the effective lifetime of the excited state is quite short with 140 fs for low temperatures and staying over 120 fs up to 150 K [Haa99]. This is explained by the presence of non radiative channels which dominates the recombination[Kra98]. A model suggesting a non radiative recombination via two channels with states situated in the gap (cf. figure5) estimates the radiative lifetime to be roughly 1 ns[Lec00]. Thus for the blue phase a fairly complete model exists at temperatures lower than 100 K.

Measurements show a large dichroic ratio in the absorption. The absorption for waves polarised along the wire is 600 times stronger than orthogonal to the chains[Lec98]. Therefore the sample has to be oriented accordingly.

Electroabsorption measurements (cf. figure 6) on the blue phase of 3BCMU show that the emission at 1.9 eV can be identified as originating from an exciton and that the states can be described by a band structure[Hor96]. The exciton has a binding energy of 580 meV and a Bohr radius of about 1-2 nm.

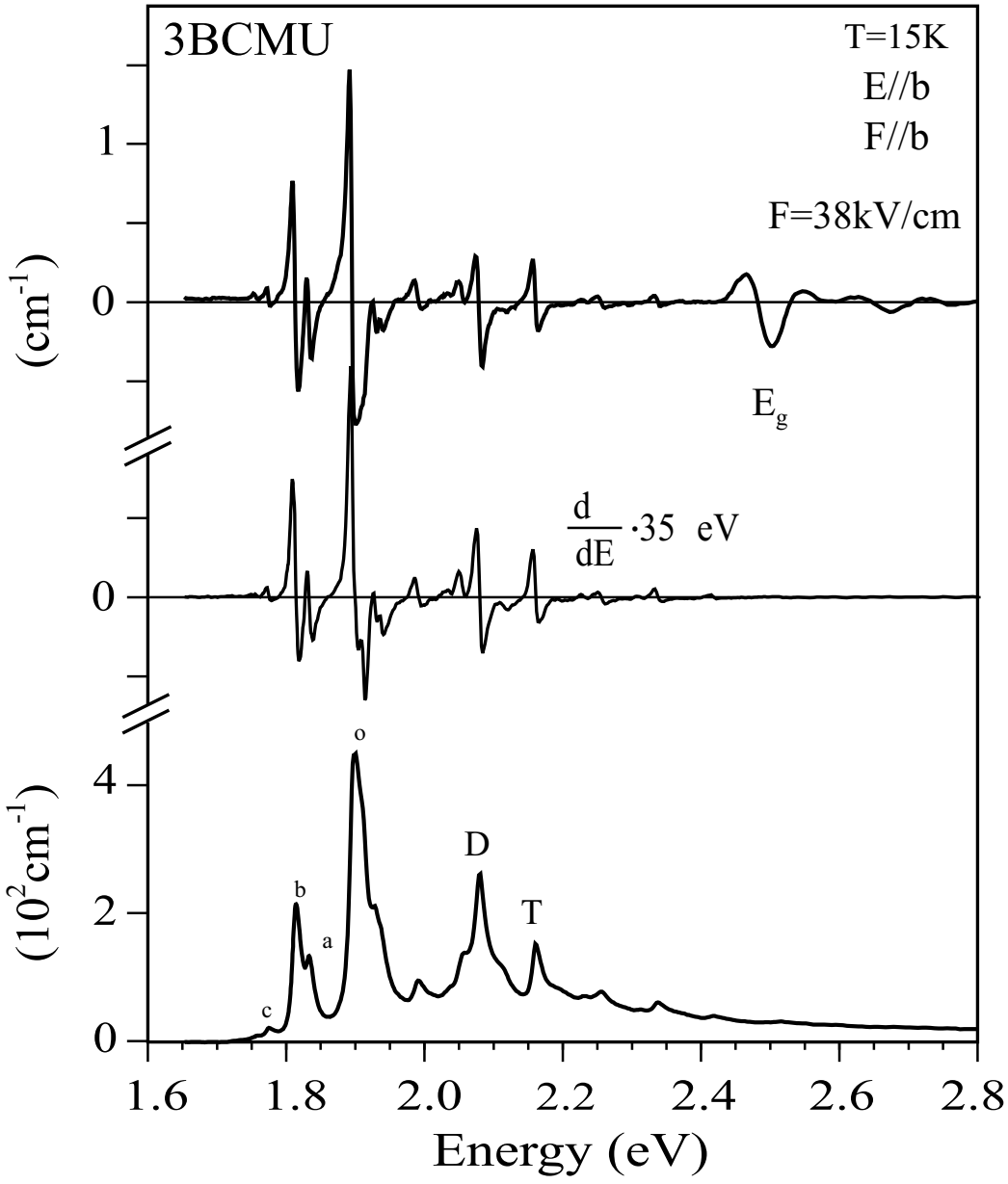

Figure 6: Electronic absorption of the exciton of the blue phase. Electronic absorption measurements for the red exciton are not possible because of the low concentration of the red phase[Hor96].

2.2.2 Red Phase of 3BCMU

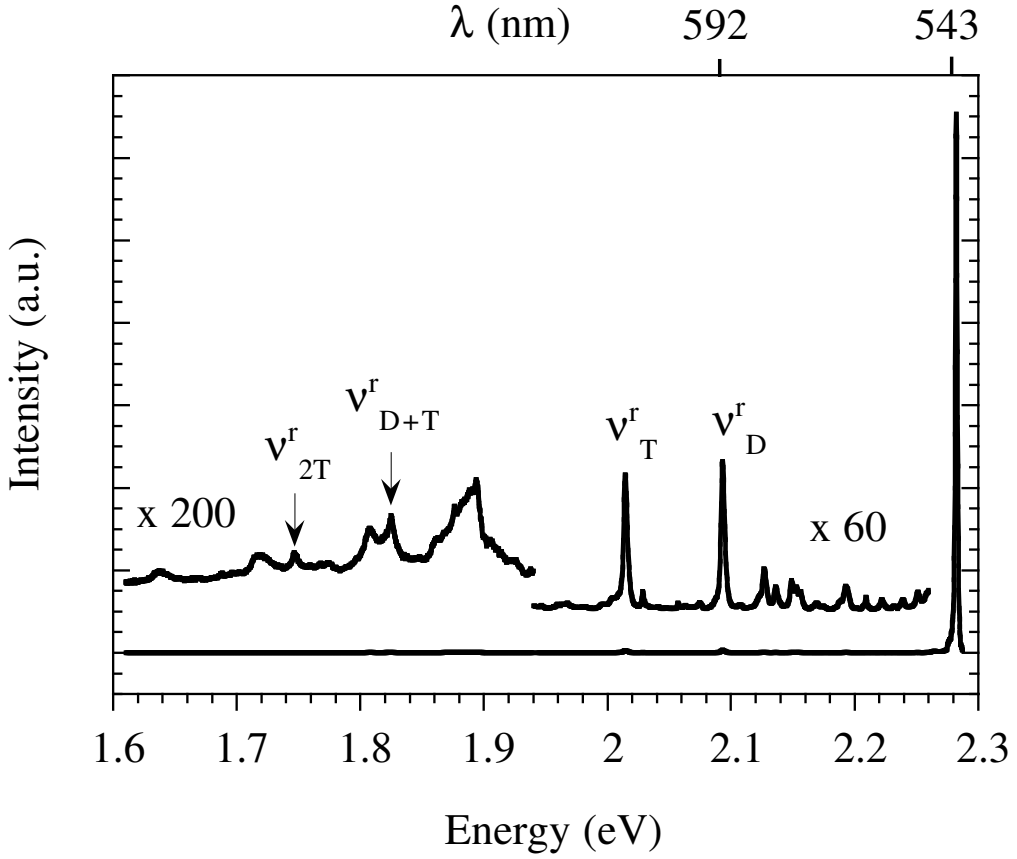

Figure 7: Fluorescence spectrum of the red phase of 3BCMU. The spectrum was taken at 15 K and the excitation was at 2.4716 eV (501.7 nm), where the D vibronic line of the red phase is situated.

The fluorescence spectrum on figure 7 of a 3BCMU crystal shows important peaks which cannot be attributed to the blue chains. Their positions, Raman frequencies and vibronic lines make it possible to identify them as signal from the red structure. 3BCMU is at the moment the only diacetylene, where the red and blue phase coexist in the form of isolated chains in a monomer matrix, i.e. in a partially polymerised cristal. Contrary to the blue phase, the red phase of an isolated 3BCMU chain has a high quantum yield of 0.3 at 20 K. This makes it possible to perform time resolved fluorescence measurements even though the red phase is minoritary to the blue phase by 10^{-3}[Lec00, Lec02]. In table 1, some principal characteristics of the two phases are listed.

	red phase	blue phase
ν_0 [eV]	2.28	1.9
ν_D [meV]	189.1	181
ν_T [meV]	267.8	261
η	0.3	10^{-4}

Table 1: Characteristics of the red and blue phase of 3BCMU. The values are valid for a temperature of 15 K.

Excitation measurements show that the red phase is a resonant emission [Lec00]. The absorption of the zero phonon line and the additional vibronic lines D and T can be found on the absorption spectrum embedded in the absorption of the blue phase (figure 4).

Time resolved measurements show that the radiative lifetime follows a law as expected for one dimensional systems. The radiative lifetime is proportional to $\sqrt{T}$ between 10 and 120 K [Lec02]. The proportionality of the radiative lifetime to $\sqrt{T}$ is a characteristic of a one dimensional system [Cit92]. The non radiative lifetime stays constant at 140-145 ps below 50 K. Above this temperature a new channel becomes active and overtakes the recombination [Lec02]. This channel could be a fission of a singlet exciton to two triplet excitons having their energy level near half of the energy of the singlet. An applied magnetic field parallel to the chains influences the efficiency of the fission in a very characteristic way, as shown on tetracene [Bou78]. In our case we expected to observe variation of about 10% in the effective lifetime for magnetic fields of 0.2 Tesla. We did some preliminary measurements but were not able to obtain a conclusive result.

Our sample is interesting in this regard simply because there are no other known systems which present this law over such a large temperature interval. One of the question which arises is the tendency below 10 K. A deviation to the square root law is expected in that the radiation time will saturate. One chapter in this manuscript will present our measurements at low temperatures (chapter 5).

In conjugated polymers the excitons are normally heavily localised. This is not the case for 3BCMU, as the conjugation length is important and the polymer is isolated and in a symmetric surrounding. The electronic structure can be described with a band structure[Dub02].

2.3 Conclusion

In this chapter the crystalline structure and the optical properties of diacetylene crystals have been presented. This proposes the red phase of the

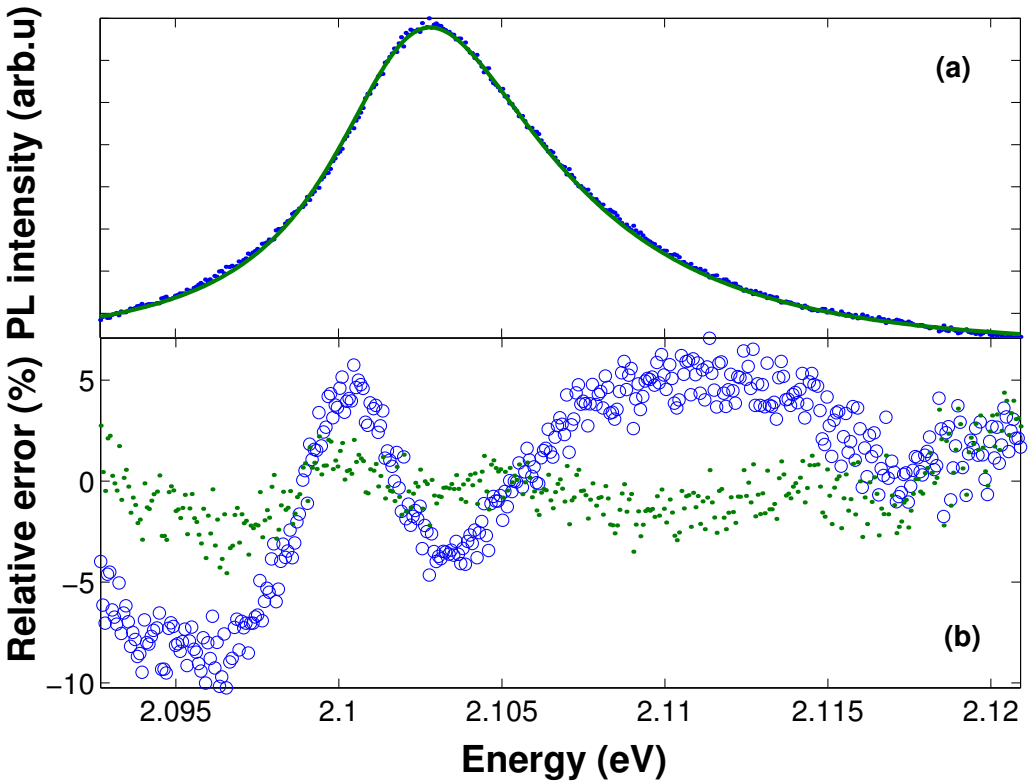

Figure 8: On Top the data and fit on the D vibronic line of the red phase are shown using a 1D band structure. On the lower part, the errors are plotted for a 1D (points) and a 2D (open circles) model.

3BCMU as a model for an ordered and isolated one dimensional system. The high quantum efficiency (η=0.3) permits to perform time resolved luminescence measurements to investigate the radiative lifetime at low temperatures. These measurements give indications about the exciton relaxation and the localisation occurring at lower temperatures (Chapter 5)

3 Experimental setup

In this section I describe the experimental setup that was used for the measurements presented in chapters 4 and 5. Pulsed laser light was used to excite the samples which were held at low temperatures by a helium bath cryostat. The luminescence was resolved in wavelength by a monochromator and a streak camera allows to draw the temporal form of the signal.

3.1 Excitation

We used a frequency doubled laser pulses of a picosecond Ti:Sapphire laser (Tsunami, Spectra physics) to excite our samples (shown in green on figure 9). The repetition rate of the laser is 80.6 MHz and the width of the pulses is about 2 ps. The wavelength is tunable from 630 to 1080 nm, covering the energies of the vibronic absorption lines of the red phase of a polydiacetylene ($\nu_D = 502\ nm$ and $\nu_T = 485\ nm$) for an optimal absorption (cf. figure 4). A part of the laser beam is used to trigger the synchronisation of the streak camera (a on figure 9). The excitation was attenuated to typically 50 to 200 μW with a variable metallic neutral density filter (b). The laser beam is focused on a spot of a diameter of 150 μm.

We were not able to find a law for the lifetime measured and wanted to be sure that their origin didn't lay in uncontrolled parameters of the excitation or in a possible drift in the position of the sample. The intensity of the excitation beam was monitored by a diode connected to an analog plotter (Phillips PM 8134) (c). The position of the sample and the laser spot on the sample were visualised with a CCD placed in the detection axis (d). The illumination of the sample was done with a green led, placed between the collecting lens and the sample to obtain best contrast (not shown on figure 9). During a series of measurements, the excitation was left untouched and when necessary the sample was brought back to its original position with micrometres screws in 3 different directions. As reference, irregularities in the crystal structure or an additionally placed piece with small enough structures (electron microscope grid, 200 mesh) were used. The precision of the position of the spot is around 50 μm.

The energy of the excitation is measured with a wavelength meter (WaveCheck cw) (e). The error in the measurement is given at 0.5 nm by the manufacturer, but we found that the value begins to be much more important at wavelength larger than 900 nm. The correct wavelength of the excitation is obtained in monitoring a reflection at a wedge (f) placed in the excitation beam. The reflection is injected into the detection axis before entering the monochromator (shown in cyan). A retardation line (g) is used to place the

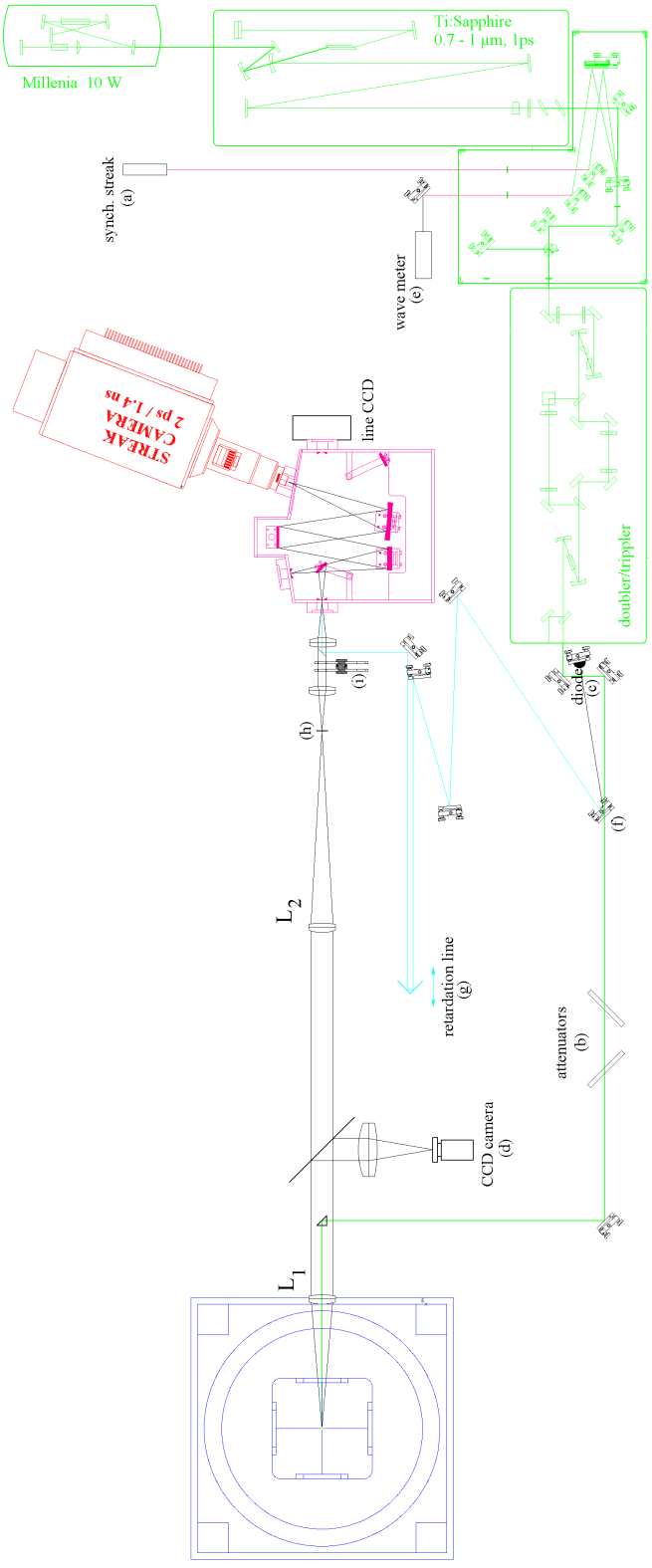

Figure 9: Scheme of the experimental setup

monitored excitation beam temporally in an useful position compared to the luminescence signal. The temporal calibration of the streak camera was done with this delay line.

3.2 Cryogenic

The sample was cooled with a cryostat (SMC TBT) (blue) which can be used either as a helium bath or as a gas flow cryostat. For temperatures below 4.2 K, the sample is immersed in helium and the temperature is controlled by the helium vapour pressure above the bath. For higher temperatures, a flow of helium is heated to a fixed temperature just before entering the sample chamber. The flow is controlled by an equilibrium of the pumping drive and the aperture of the valve situated between the helium reservoir and the temperature control unit. Temperatures from 4.2 to around 7 K are difficult to control with this type of cryostat because at these temperatures the control parameters are sensitive.

We observed a variation of the position of the end of the sample holder. The sample holder has a length of about 80 cm and the helium flux creates a temperature gradient along the holder. The dilatation of the whole holder depends on this temperature gradient, which varies for different temperatures and flows and is not controlled. We have also observed a smaller lateral displacement which is probably due to the inhomogeneity of the holder.

For the measurements in function of the excitation energy, a closed cycle cryostat (CTI-Cryogenics) was used at a fixed temperature of 15 K. As the spectral position and temporal response of the luminescence showed to be independent of the excited position on the sample, spatial stability was not of concern. The helium cycle pump vibrates the cryostat and as a consequence the measurements are a mean value of a region of about 200 μm.

Usual methods to glue samples to the holder are not usable because the solvents in the glue attack organic materials. The material used to fix the sample needs to be non fluorescent and have a good thermal conductivity for the closed cycle cryostat, where the temperature is regulated through the sample holder. A grease (Dow Corning 340, heat sink compound) where carbon was added for better thermal conductivity verified all the conditions requested above.

3.3 Detection

The luminescence of the sample was collected by a lens of 80 mm focal length (L_1) and sent through a lens of focal length of 300 mm (L_2), which focalises the luminescence on a spatial filter and magnifies the image by a factor of

3.75. The filter is a pinhole of 25 μm (h) and selects the central zone of the excitation spot on the sample to guarantee a signal from a uniformly excited region. We will come back later in the text (page 18) to the choice of the size of the pinhole. Before entering the monochromator (magenta), the detection passes a coloured glass filter (Schott: OG515, 3 mm) (i), which cuts diffused laser light from the detection. At the same position neutral density filters are placed to control the intensity of the measured signal. The intrinsic resolution of the grating in the first order is given by the following relation (for the parameters, see table 2):

$$\Delta\lambda = \frac{\lambda}{NL} \tag{1}$$

λ	wavelength of the luminescence	around 500 nm
N	grooves per mm on the grating	150 mm^{-1}
L	width of the grating	60 mm
w	width of the entrance slit	25 μm
F	focal length of the monochromator	250 mm
α	angle of incidence to the grating	<90°

Table 2: Characteristics of the monochromator

The resolution will be slightly worse because the diffraction grating is not illuminated over its complete width. In our case the instrumental resolution (e.g. the bandpass B) is dominated by the dimension of the entrance slit, which was chosen equal to the size of the pinhole. The bandpass can be calculated by the following formula:

$$B = \frac{w \cos\alpha}{NF}$$

In our case, this gives a spectral resolution of about 0.5 nm (2.2 meV).

At the exit of the monochromator a streak camera (Optronis, Hamamatsu) is placed (red). The camera has a temporal resolution of 2 ps. In our situation the resolution depends mainly on the synchronisation of the camera. An internal oscillator is accorded to the repetition rate of the laser by a diode measuring the laser pulse. Irregularities over a small number of pulses remain undetected and have a bad impact on the resolution, whereas slow continuous drifts in the frequency of the laser can be detected. The repetition rate of the laser is set by an external frequency generator (adret electronique, generateur VHF). To detect any jitter, the laser pulse is monitored on the streak camera image and gives us a control of the stability of

the synchronisation and the laser and the exact energy of the excitation (cf. Fig 22). The total temporal resolution of the setup is given by:

$$\Delta t = \frac{NL}{c}\lambda \tag{2}$$

and when comparing (2) with (1) one sees that the spectral and temporal resolution are directly related:

$$\Delta t \Delta E = \Delta t \Delta \lambda \frac{hc}{\lambda^2} = \frac{\hbar}{2} \tag{3}$$

For a grating of 150 grooves/mm, the width of the laser is measured at 15 ps and is equal to the resolution for the setup.

There is also a balance to be found between the size of the measured spot on the sample and the spectral resolution. As showed above, the resolution in our setup is limited by the dimension of the entrance slit of the monochromator or alternatively by the diameter of the pinhole (h). A diameter of 25 μm leads to a spectral resolution of 2.2 meV. To illuminate the grating in the monochromator over the full width, the aperture of L_2 has to be fixed. This leads, with the diameter of the lens of 2 inches, to a focal length of 300 mm. The ratio of the focal length of the two lenses L_2 and L_1 set the magnification of the sample on the pinhole. We are interested to have a focal length as small as possible for the lens L_1, because we want to collect the most luminescence. Also the diameter of the laser spot on the sample is reduced. The cryostat limited the focal length to 80 mm, which leads to a magnification of about 4. In other words, the diameter of the spot on the sample which passes the pinhole has a diameter of 6 μm. This has to be compared to the diameter of the excitation beam, which is mentioned above as 150 μm.

The size of the pinhole could also impact the temporal resolution. The camera from Hamamatsu images a pinhole of 25 μm on about 6.5 pixel on the temporal axis, which corresponds to 4.9 ps in the configuration we used. In our case it is not the diameter of the pinhole which limits the temporal resolution, because the 4.9 ps are clearly shorter than the resolution of 15 ps. Nevertheless for pinholes larger than 45 μm, the pinhole fixes the spectral and the temporal resolution on the streak camera of Hamamatsu.

The transfer of the wavelength resolved signal to the streak has two problems. First, the exit plane of the monochromator is not planar. A compromise on the sharpness over the spectrum has to be taken. In most of our measurements this was not really of concern, because the signal of the zero phonon line covers 1/20 of the height of the image. Second, only the central wavelength benefit from the total aperture of the entrance optics of the camera

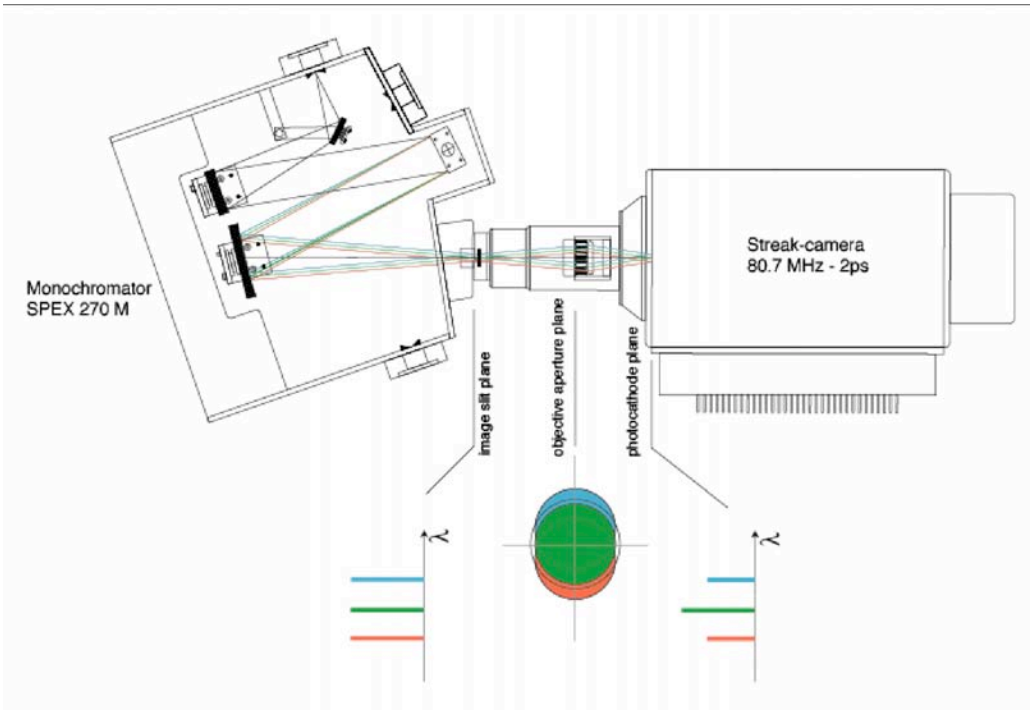

Figure 10: Figure showing the transfer of the signal between the monochromator and the streak camera. The aperture of the camera cuts off signal of the colours which are not centred.

(cf. Fig 10). For spots placed outside the centre of the axis, the more they are distant to the centre the more of signal is blocked by the aperture of the camera.

The streak camera is used to obtain a temporal response of the signal. The photons are transformed by a photo-cathode into electrons which are deflected by an electromagnetic field which varies in function of time. The electrons hitting the phosphor layer are transformed into photons which are read by a CCD. At this stage the signal is resolved on the horizontal axis by its wavelength and on the vertical axis by its time. The geometry and temporal function of the electromagnetic field is engineered to have a linear response on the time axis. Depending on the manufacturer, the signal is amplified by accelerating the electrons in a multi channel plate (MCP) either in the same tube, where the temporal deflection is done (Hamamatsu), or in an additional unit placed between the phosphor layer and the CCD (Optronis). To reduce the noise and also assure a linear response in intensity, the accumulation of the signal is done in photon counting mode. There are two kinds of noise added to the signal, one generated in the amplification and photon/electron

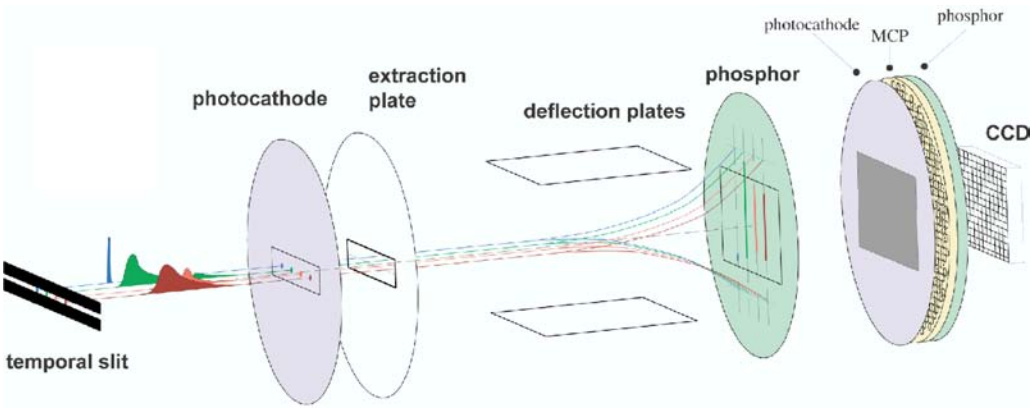

Figure 11: Scheme of a streak camera. The light enters on the left and is transformed by the photo-cathode in electrons, which can be deflected to obtain a temporal resolution. The signal is detected by a CCD camera after transformation by a phosphor layer. The multi channel plate (MCP) amplifies the signal.

transformation process* and a second generated by the read-out of the CCD camera. Only the second one can be eliminated. To differentiate the signal from the read-out noise, the amplification in the MCP of the signal is set to its maximum and an offset is placed above the level of the noise. The linear response of the signal is guaranteed by only counting one event every pulse. Therefore a relatively fast read-out frequency of 10 Hz is used and a grey filter placed at the entrance of the monochromator adjusts the intensity of the entering signal. For the interpretations we want to do, a dynamic of 3 order of magnitude is needed, which requires an integration time of around 20 minutes. This shows that a balance has to be found between the stability of the measurement and the dynamic of the signal.

3.4 Setup for Absorption Measurements

The absorption measurement were performed in Paris at the Groupe de Physique des Solides with a spectrometre by Cary. White light was separated in two beams, one for reference and the other was sent through the sample to measure the absorption. The absorption is thus measured by transmission. A linear polarisator was placed in each beam, and the orientation of the filters were set to be parallel to the polymer chains to have a maximal absorption. An opening of about 2 mm in the sample holder defines the diameter of the spot. The sample was cooled by helium in an open cycle cryostat.

*This noise is thermaly activated. Therefore, in cameras optimised for IR detection, the photocathode is usually cooled.

4 Absorption and Excitation Measurements

In this chapter the results of the absorption and excitation spectra of the red phase of 3BCMU are presented. We found a relatively small Huang-Rhys factor of about 0.04. The band edge seems to be suppressed as it has been shown for the blue chain [Hor96].

4.1 Absorption of the Red Phase

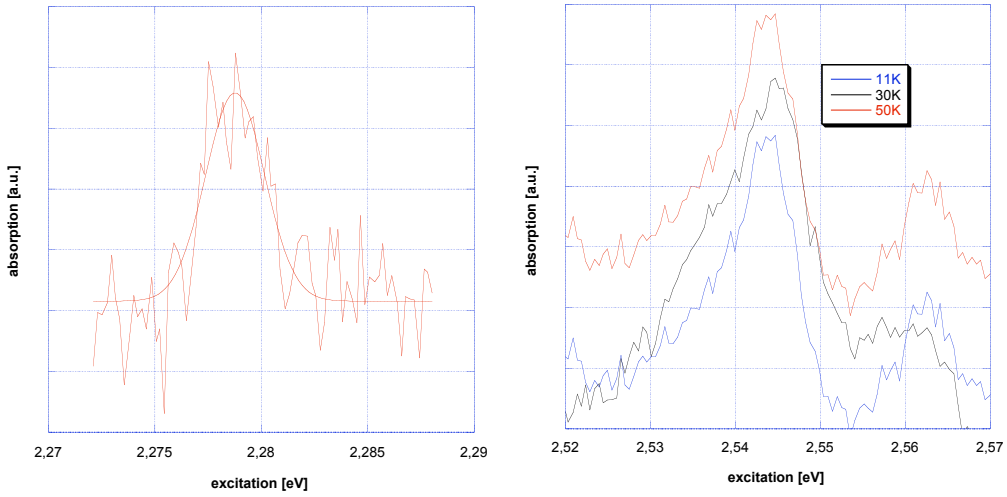

(a) zero phonon line: ν_0

(b) vibronic line T: ν_T

Figure 12: The absorption intensity of the zero phonon line at 11 K and of the T vibronic line for three different temperatures of the red phase. The intensity axis are not in scale because for the ν_0 line two spectra and for the ν_T line 6 spectra were added to obtain the final spectrum.

Absorption measurements of the zero phonon line and the line of the vibronic phonon T of the polymer backbone are presented in figure 12. The absorption measurements of the T line are interesting, because in the experiment described in chapter 5 we excited in resonance to the T vibronic line. The position of the T vibronic absorption line and the width should not change considerably to ensure that the measurements at different temperatures are comparable. As can be seen on figure 13, the intensities of the absorption lines of the red chains are orders of magnitude smaller than the absorption of the blue chains. Several spectra were added to obtain a

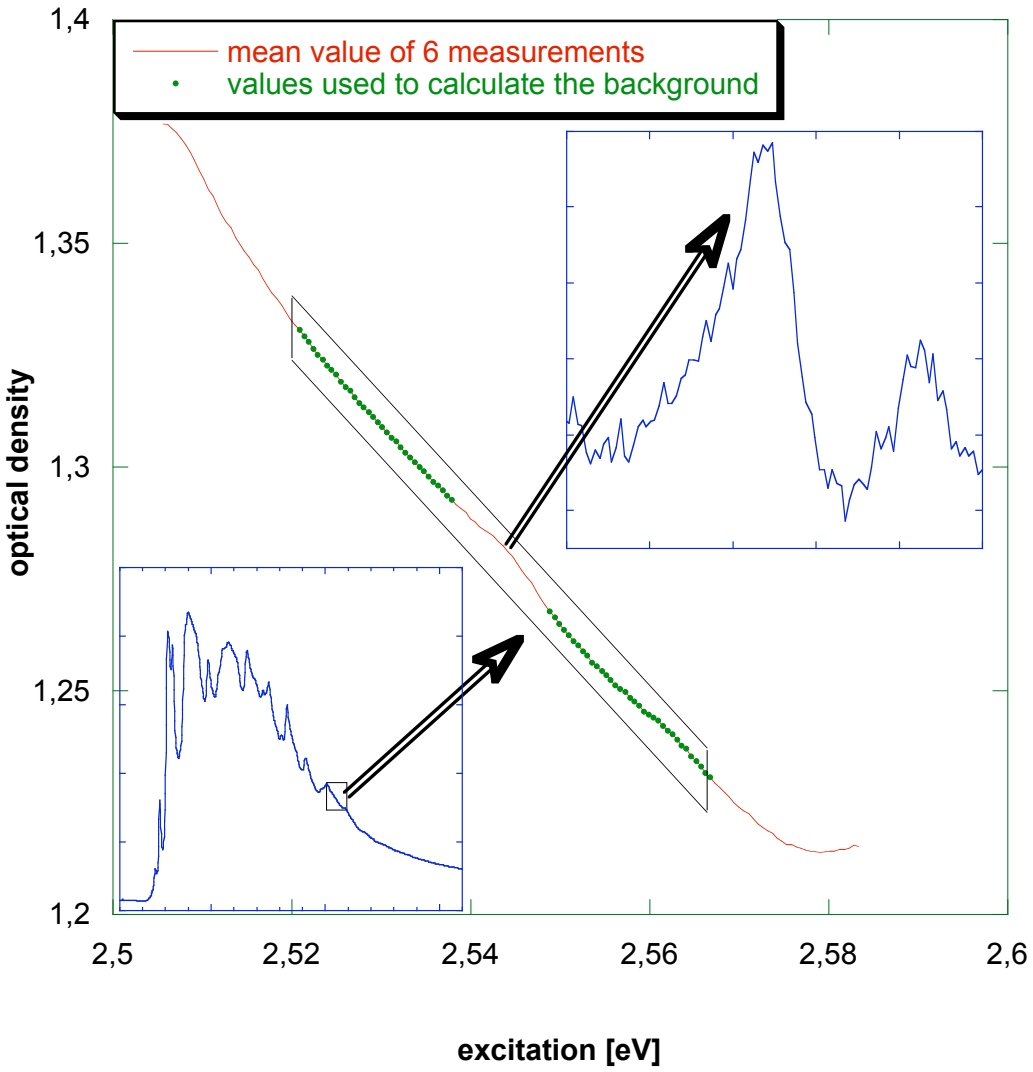

Figure 13: The procedure to obtain the absorption spectrum of the T line of the red chains is shown. A polynome of second order is substracted from the total absorption (red line). The polynome is fitted to the measurements shown as dark green dots.

significant signal. The shape of the absorption lines was obtained by subtracting the absorption of the blue phase fitted by a polynome of second order as shown in figure 13. The form found for the absorption lines is thus depending on the subtraction of the background.

The zero phonon line shown in figure 12(a) was fitted by a Gaussian function. Fluorescence measurements on a single red chain at 10 K have a width of around 0.6 meV [Dub04]. The measured linewidth in figure 12(a) is clearly inhomogeneous. Comparison of fluorescence measurements on a single chain and measurements with a spot of about 100 μm, lead to the conclusion that the homogeeous linewidth, which increases with T, becomes larger than the inhomogeneous one at around 30 K.

We measured the following maximal intensity I, spectral position E and linewidth Γ:

I	=	$1.71{\cdot}10^{-2}$	$\pm 1.4 \cdot 10^{-3}$
E_0	=	2.2788	$\pm 1.3 \cdot 10^{-4}$eV
Γ_0	=	3.26	$\pm$0.32 meV

For the T absorption line the linewidth is supposed to be homogeneous. Previous measurements show that the linewidth of the absorption and of the fluorescence of the D line of the red chain are nearly identical and measure about 5 meV [Lec02, Figure 2]. This is in accord with the relaxation time of around 40 fs measured for the blue chain when exciting at the D line [Haa99]. On the other side the inhomogeneous broadening is expected to be similar to that of the zero phonon line, therefore smaller than the homogeneous width. The width of the state compounded by an exciton and a T phonon would be in the first order the sum of the width of the exciton and the phonon. The width of the exciton was estimated above and is about 3.3 meV. The inhomogeneous width of the T phonon is certainly smaller, as the phonon is located on the carbon triple bond. The rigidity of this bond depends little on the surrounding. Therefore the contribution of the phonon to the inhomogeneous width is expected to be small. The T absorption line was thus fitted by a Lorentzian function.

It is clearly visible that the lower energy flank of the T line can not be fitted by a single Lorentzian function. The spectrum was fitted by two Lorentzian functions, where the more intense peak was attributed to the T line (the fits are shown on figure 21). The reason of this choice will be explained in another paragraph (4.5.1) on page 38. In the following table the values for the Lorentzian fit on the T absorption line are presented for three different temperatures:

	11K	30K	50K
I	$4.2 \cdot 10^{-3}$	$6.0 \cdot 10^{-3}$	$4.1 \cdot 10^{-3}$
Γ_T[meV]	5.8±1.2	7.0±1.0	7.0±1.4
E_T[eV]	2.5440±3·10^{-4}	2.5452±3·10^{-4}	2.5471±4·10^{-4}

The intensities given above are normalised to an identical integration time. The table above indicates that the position and linewidth do not change considerably in the temperature interval in which we performed our measurements. We explain the differences between the three spectra by the errors introduced by the subtraction of the background.

Note that we were not able to extract the D absorption line because it was hidden by the flank of an absorption line of the blue phase. The zero phonon and D line were already characterised by previous measurements on another sample [Lec98, Lec02]. This was possible because the position of the excitonic lines can vary slightly from one sample to another. Therefore, for certain samples, the D absorption line of the red chain is not masked by a more important peak of the blue chain. The position of the D absorption line has been measured at 186 meV above the zero phonon line with a linewidth of about 5 meV. As the parameters of the zero phonon line are known, we contented ourself with an accumulation time 3 times shorter in respect to the T line.

At 2.5626±2·10^{-4} eV (figure 12(b)) there is a smaller peak visible, which has a comparable width (3.3±0.4 meV). In excitation measurements a peak at about the same energy (20 meV) above the zero phonon line is observed [Lec00]. This peak is therefore a phonon replica corresponding to the combination of the T phonon with a phonon at 20 meV.

The excitation of the red chains at the energy of the T absorption line is thus suitable for our experiments.

The fact that the absorption spectrum of the red phase is largely dominated by the spectrum of the blue phase, makes the direct measurement of a complete absorption spectrum impossible. In the following section, an excitation spectrum measurement of the red chains is presented. We will show that with this spectrum, the absorption modes can be unambiguously attributed to the vibration modes, except for the satellite peak on the low energy side of the T absorption.

4.2 Excitation Measurements

4.2.1 Presentation of the Results

The measurements were performed with the setup described in chapter 3 using the closed cycle cryostat, regulated at a temperature of 15 K. The

large interval of excitation energy made it necessary to change the cavity mirrors of the excitation laser. The resolution in the excitation energy was imposed by the availability of stable modes of the laser, which were spaced by about 2-4 nm (10-20 meV). This gives the possibility to plot the global view of the spectrum but the low resolution results in rather approximate positions and widths of the peaks. The spectral width of the laser is clearly below the resolution of the setup and estimated at $\Delta E \approx 200\ \mu eV$[†]. The measurements were done on different points on the sample because of the change of the laser mirrors, which has as consequence that the laser beam has a different pointing. The spot on the sample was chosen to maximise the intensity of the signal. As the concentration of red chains can change from site to site, an unquantifiable error in the intensity of the luminescence is introduced. This can to a certain extent be obviated by scaling two different measurements in the wavelength region where they overlap.

Figure 14 shows a graph of the intensity of the zero phonon line in function of the excitation energy. The intensities of the three different segments were obtained with different mirror sets for the laser cavity, which are optimised to the wavelength interval. For higher energies, the excitation intensity had to be increased from 10 μW to 50 μW to obtain still an interpretable signal. Because of the different excitation intensities and the changes of the cavity mirrors, the respective intensities are delicate to compare. The intensity was either taken as the temporal maximum of a window of 4.4 meV around the zero phonon line (continuous lines in figure 14) or as the integral over the whole timescale of 800 ps (discontinuous lines). The two plots show nearly the same relation. The absorption of the blue phase varies by a factor of 5 over the excitation energy interval. Therefore the intensities were corrected by the absorption factor of the blue phase, which can be seen on figure 4. The width of the D and T line are smaller than 15 meV (resp. 19 meV), considering that the distance between to energies in the excitation is between 10 and 20 meV. This is consistent with the known absorption widths of a few meV.

We verified that there was no contribution from Raman scattering either from the blue or red phase. The Raman scattering would be visible as a signal with a temporal width of the order of the laser pulse. The Raman scattering at the energy of the blue D phonon has been measured to have an intensity 1:750 of the red zero phonon line [Dub04]. With the accumulation times used for our measurements, the Raman scattering disappears in the noise.

We found no notable differences in the recombination times of the zero phonon line.

[†]The pulse width of the laser is about 2 ps. $\Delta E\,\Delta t \geqslant \hbar/2$ gives $\Delta E \geqslant 165\ \mu eV$.

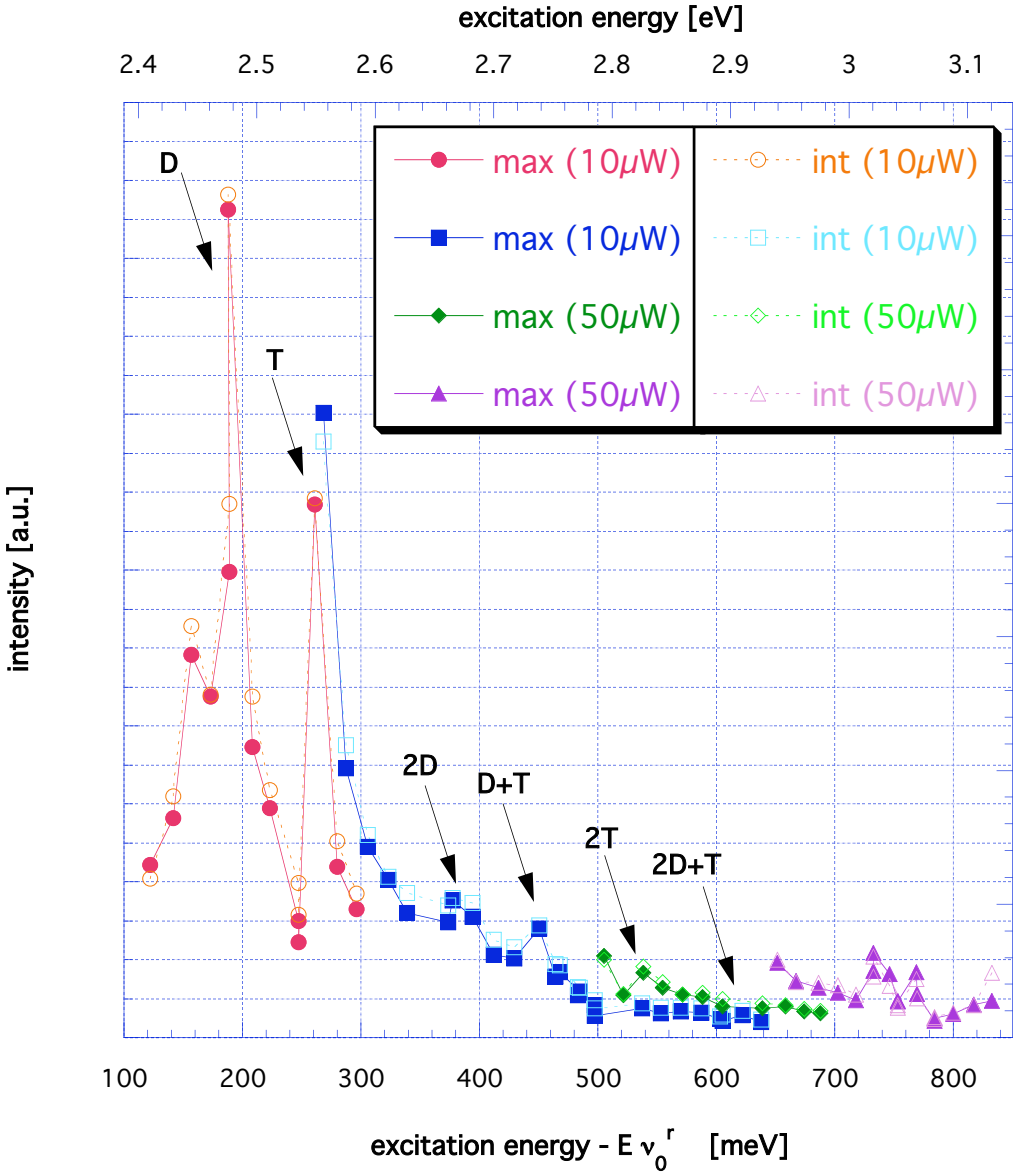

Figure 14: Intensity of the zero phonon line (2.28 eV) at 15 K in function of the excitation energy. The x axis shows the difference of the excitation energy to that of the zero phonon line. The different colours show different setups of the cavity mirrors of the laser. Filled points show the maximum of the temporal signal, empty points show the integral over the temporal window.

4.2.2 Discussion of the Excitation Spectrum

For the case where all the excited states created by the absorption are found again in the exciton state near the bottom of the band, the excitation and absorption spectra are identical. This remains true if a fixed fraction independent of the excitation energy contributes to the luminescence. Suppose now that an additional channel becomes active, when exciting above or exactly at a certain energy. If this channel does not pass through the exciton state mentionned above, the quantum yield and thus the measured luminescence intensity becomes smaller. In this case, one would see a decrease in the excitation spectrum intensity that would be absent in the absorption spectrum. The maxima remain at the same energies for the two spectra, if they are of enough intensity in the excitation spectrum. As an example for such a process, the fission of a singlet exciton in two triplet excitons could be given [Kra98].

The peaks can be identified as the fundamental line of the red chain with a combination of the vibronic modes of the carbon bonds. In the following table, the energies of the multiple of the D and T vibronic lines are reported for the absorption, the excitation and the fluorescence spectra:

	absorption	excitation	fluorescence
D	186	188	189.1
T	265	265	267.8
2D		378	
D+T		451	456
2T		538	536
3D		570/579	
2D+T		624	

The energies estimated for the 3D and 2D+T are only a tentative attribution. The intensities and therefore the exact determination of the modes are less accurate because of the sensitivity of the setup, which degrades below 450 nm. Also the ratio of the signal to the noise is smaller at higher modes. The energy of the T mode for the absorption was estimated at 265 meV.

A comparison of the absorption, fluorescence and excitation spectra shows that the distance in energy of the vibronic lines to the zero phonon line are within the error of the measurements (cf. figure 15 for a comparison of the fluorescence and excitation spectra). The fluorescence spectrum was obtained by taking into account only the signal some ten of picoseconds after the initial luminescence signal a time resolved spectrum. In this way, the luminescence signal of the blue fluorescence is eliminated, as its lifetime is about 130 fs [Haa99]. Note the absence of the 2D line in the fluorescence

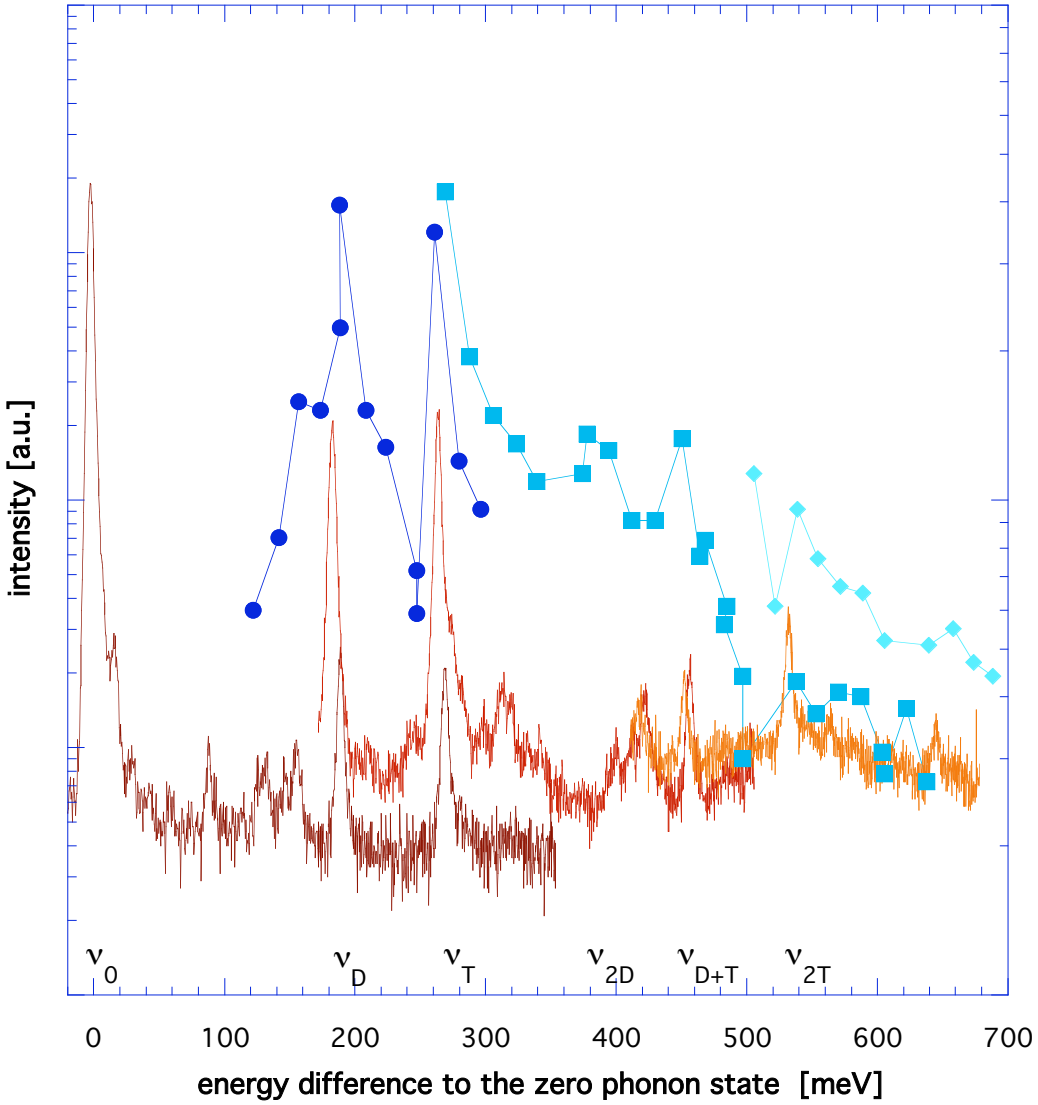

Figure 15: Comparison of the fluorescence spectrum to the excitation absorption spectrum (lines with dots). On the bottom are marked the positions of the respective phonon lines.

spectrum around 1.91 eV, which can be explained by the reabsorption by the blue zero phonon absorption line. A comparison to the absorption spectrum is only possible to a certain degree for the zero phonon and the first vibronic T lines (cf. figure 12(b)). The other resonances have a signal too weak to be visible next to the absorption signal of the blue phase.

The difference between the sum of the single vibration energies and the energy of a composed mode (for example $2E_T$ and E_{2T}) can be explained by a small anharmonicity of the vibration modes.

The relative intensities of the modes of the fluorescence and excitation spectra are comparable. Contrary to the fluorescence spectrum, which has a nearly constant background, the background of the excitation spectrum is decreasing for higher energies. This background is possibly due to vibronic transitions involving multiple phonons, but the data are not of sufficiently high resolution to allow further discussion.

4.3 Huang-Rhys Factor

The Huang-Rhys factor S gives an information about the coupling strength of the excited state to the ground state [Fit68, p. 293]. We give a short explanation how the Huang-Rhys factor relates to the transition probability between the fundamental and a vibrational level of an excited state.

We assume two non degenerate electronic levels a and b. q is a general spatial variable in the lattice. Considering only the electronic motion, the harmonic potentials for the levels a and b are

$$E_a = \frac{1}{2} M\omega^2 q^2$$

and

$$E_b = \frac{1}{2} M\omega^2 q^2 + E_{ab} - A\hbar\omega\sqrt{\frac{M\omega}{\hbar}}q$$

where M is the effective mass of the mode and E_{ab} the difference in energy between the vibrational mode of the excited state to the vibrational mode of the ground state. A is a measure of the strength of the linear interaction which displaces the equilibrium position. The energy eigenvalues of the vibrational modes are

$$\epsilon_{am} = (m + \frac{1}{2})\hbar\omega$$

for the ground state, and

$$\epsilon_{bn} = (n + \frac{1}{2})\hbar\omega + E_{ab} - \frac{1}{2}A^2\hbar\omega$$

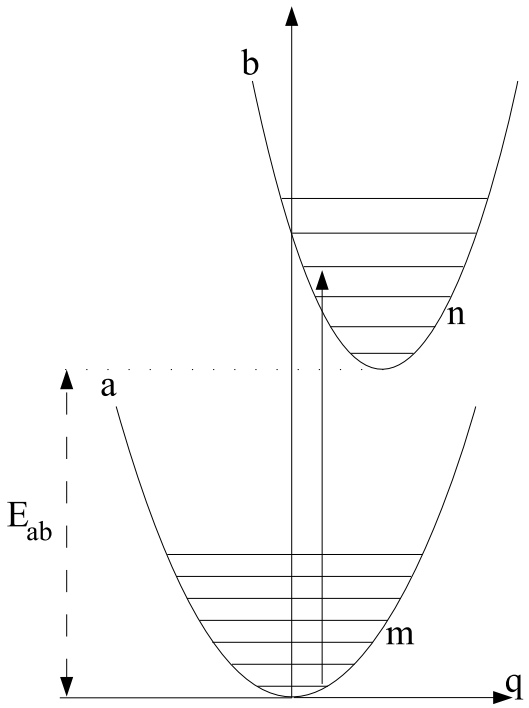

Figure 16: Energy diagram of the ground (a) and excited (b) electronic states. The levels of the vibrational states are shown by horizontal lines.

for the excited state. Assuming $\Psi = \psi_a(\mathbf{r}, q)\chi_{am}(q)$, which corresponds to separation of electronic and nuclear motion, the transition probability is written:

$$|< \Psi_{bn}|\mathbf{r}|\Psi_{am} >|^2 = |< \psi_b\chi_{bn}|\mathbf{r}|\psi_a\chi_{am}\rangle\,|^2 = |< \psi|\mathbf{r}|\psi >< \chi|\chi >|^2$$

We suppose that the electronic dipole moment is independent of the vibrational mode. The transition probability W_{nm} is proportional to the vibrational overlap integral.

$$W_{nm} =< \chi_{bn}|\chi_{am} >= \exp\left(-\frac{A^2}{4}\right)\sqrt{\frac{m!}{n!}}\left(\frac{A^2}{2}\right)^{\frac{1}{2}(n-m)} L_m^{n-m}\left(\frac{A^2}{2}\right)$$

L_m^{n-m} is a Laguerre polynomial. Finally, rewriting the transition probability with $S = A^2/2$, the Huang-Rhys factor, we obtain

$$W_{nm} = \exp(-S)\frac{m!}{n!}S^{n-m}\left(L_m^{n-m}\right)^2$$

At low enough temperature, where the only occupied initial level is $m = 0$

$(L_0^{n-0}(S) = 1)$

$$W_{n0} = \frac{S^n}{n!} e^{-S}$$

In our case we will compare the intensities of the vibrational modes D and T. The lowest vibrational mode considered is D at an energy of 189.1 meV, which corresponds to a temperature of 2194 K. The measurements we performed are thus correctly described by the relation presented before.

In the following table, we present the Huang-Rhys factors for the transitions noted in the first column. The values presented are the ratio between the absorption band surfaces, which was simply approximated by the ratio of the maximal intensities. For the ratio of the ν_T and ν_0 lines, as their line widths are different, the surface was calculated as the product of the maximal intensity and the width.

	ν_T/ν_0	ν_{2T}/ν_T
absorption	0.05	-
excitation	-	0.04
fluorescence	0.011	0.05

These values are comparable and are certainly in the range of error of the measurements. Given the incertainties in the different measurements, the factor for the fluorescence is the most accurate.

S has also about the same value for the 3 different spectra, which is usually the case for small factors, indicating a large overlapping of the ground state and excited wave function.

4.4 Band Edge of the Exciton of the Red Chain

The binding energy of the exciton of the red chain is unknown. Its value is expected to be large because of the following two reasons: First, the electronic correlations in conjugated polymers are important and second, the lateral confinement of the excitons on the chain is given by the dimension of the electronic orbit, thus at least one or two order of magnitudes smaller in dimension than for example AlGaAs/GaAS structures.

For the exciton of the blue phase the binding energy was measured by electroabsorption [Hor96]. Its value was determinded as 580 meV. Unfortunately this measurement is not possible for the red phase of 3BCMU. As the absorption of the red phase is much smaller than the blue phase, the resulting signal of the red free carriers is vanishing small.

For other polydiacetylene crystals of the blue phase the absorption signal is intense and well resolved. For these systems the binding energy of the

blue exciton has been measured at around 500 meV [Wei92]. There exist some crystals in the red phase, but their electroabsorption signal is weak and poorly resolved. There is a spectrally large and weak signal visible at around 600 meV above the energy of the exciton in the new PDA crystal TCDU [Sch]. This signal was attributed to the band edge and the attenuation explained by disorder [Wei97]. It was shown on weakly polymerised crystals of 4BCMU for the blue phase that disorder can indeed blur the signal of the band edge [Ber04].

Another approach to locate the band edge are absorption measurements. In an absorption spectrum of a one dimensional system one expects to see a continuous absorption intensity for energies higher than the band gap. In one dimension, the continuous line would follow the joint density of states of one dimension of the form of $1/\sqrt{E}$. At the the band edge the so called Van Hove divergence would manifest itself by a very sharp peak in the spectra. This image is based on free carrier properties of one dimensional systems and it ignores any disorder-induced and Coulomb-correlation effects. Electron-hole correlation introduces the exciton lines in the spectra below the band edge and smooths the above mentioned singularity. Contrary to two or three dimensional structures, the Sommerfeld factor (Coulomb enhancement factor), defined as the absorption intensity ratio of the unbound continuum exciton to the free-electron-hole-pair above the band edge, is smaller than unity (cf. figure 17, [Ros96a, Ros96b]). Experimental observations of the band edge are rare for one dimensional systems. For T-wires in a AlGaAs-GaAs compound the band edge has been seen [Aki03], but the signature of the band edge is very small (cf. figure 18).

In another theoretical approach, the attenuation of the band edge is also predicted, provided the electronic correlations are of enough importance [Bae92, Abe89].

For 3BCMU, the band edge is not visible for the blue phase in the absorption spectra [Spa94, Hor96].

Because of the domination of the blue phase over the red phase in absorption, it is hopeless to try to localise the band edge of the red phase in an absorption spectrum. Nevertheless excitation spectra could give informations about the position of the band edge for the red phase. The high quantum yield of the red phase makes it possible to obtain an excitation spectrum. In the absence of channels which become active at higher energies than the band edge the absorption and excitation spectra should be similar (cf. page 27).

Our measurements do not have any evident signature of a band edge of the red phase. Around 580 meV, no change of the intensity due to the free carriers is visible. Looking at the overall aspect of the spectrum, the background seems to become more important at around 270 meV and diminishes for

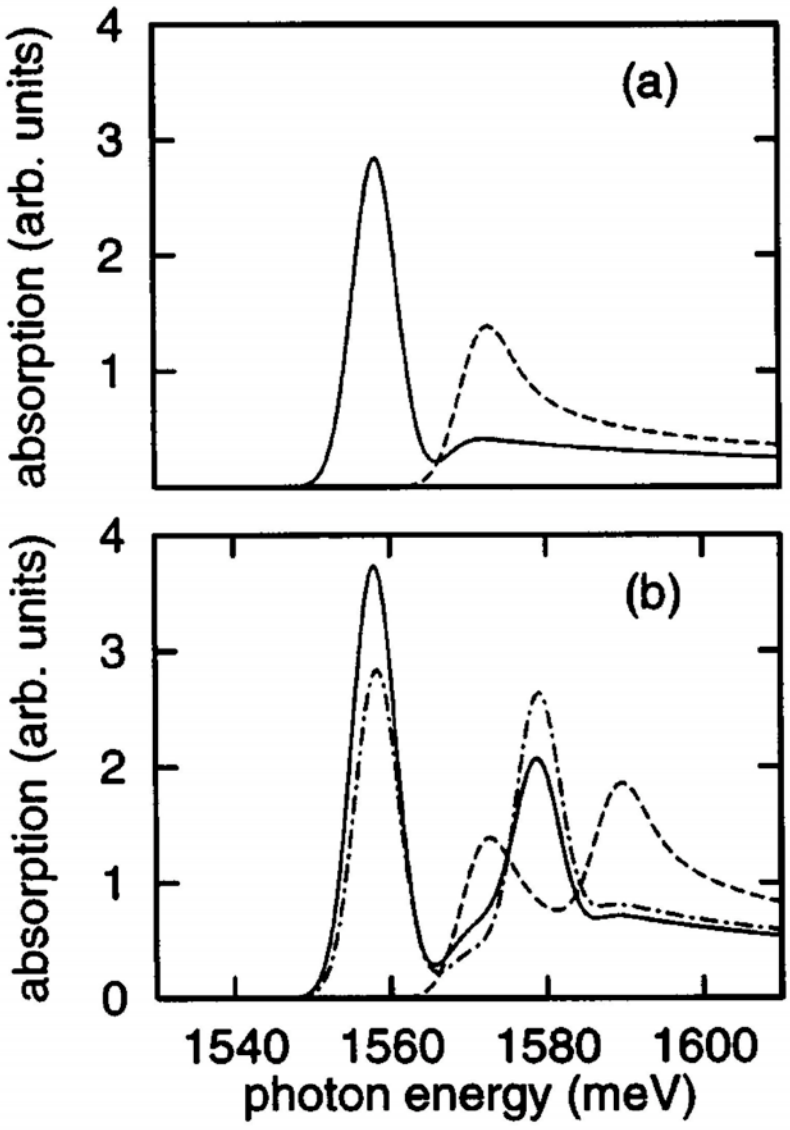

Figure 17: Simulated absorption spectrum of a V-shaped quantum wire with a thickness of about 10 μm. The dashed lines show the calculated absorption spectrum for free carriers. When electron-hole Coulomb interaction is included, the band edge is attenuated (solid line). In the figure (a), only the first wire subband is included, whereas in spectrum (b) the two lowest subbands are taken into account [Ros96a].

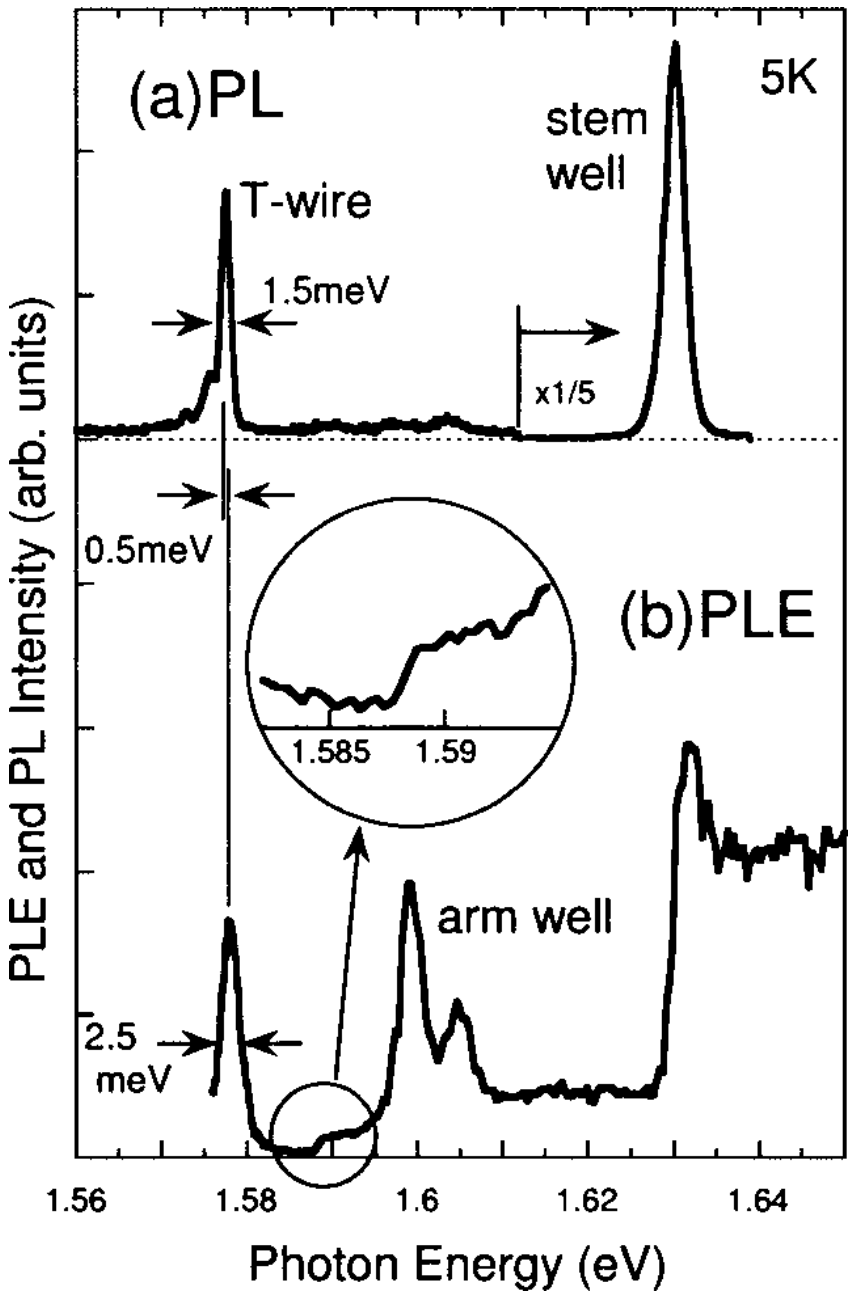

Figure 18: Photoluminescence (PL) and excitation (PLE) spectra of a T quantum wire. The step visible in the circular inset of spectrum (b) is attributed to the band edge [Aki03].

higher energies, as expected for the signal of the free carrier. This would place the band edge nearly at the same energy as the T vibronic line. A verification would be to compare the intensities on the two sides of the T vibronic peak, where the background at 250 meV should be smaller than at 340 meV. The spectrum presented here does not permit to do this verification because the two regions were not measured during the same series and it is impossible to compare directly their respective intensities. Furthermore the resolution of the excitation width of about 15 meV, due to the spectral separation of stable modes of the laser, make it difficult to localise the intensity minimum between the D and T line. Note that a confirmation of a band edge below 300 meV, that is a rest exciton binding energy $E_b \lesssim 300$ meV, half the blue exciton value, would come as a surprise and a theoretical challenge.

A possible explanation for the invisibility of the band edge and the signal of the free carrier would be that at energies above the band edge an additional channel opens. If this channel is efficient enough, the signal would disappear. Exciting at an energy higher than the band edge, an electron hole pair is created. If the creation time of the exciton is long enough, a spin relaxation of either the electron or hole are possible and the created exciton would be of triplet symetry. Those exciton would not recombine radiatively. Another possibility would be that the exciton creation time becomes comparable to the exciton recombination time. The temporal profile would change and be characterised by a visible rise time and an exponential decay. Contrary to the case of the triplet excitons, the integrated intensity of a cycle would remain constant. We found no differences in the temporal profiles of the luminescence. Therefore, if electron-hole pairs are created the formation time of the singlet exciton is either very short, or much longer than the recombination time. In the first case, electron-hole formation and decay will not affect the luminescence, since the time is too short for any spin relaxation to occur. In the second case, the corresponding emission is buried in the long time noise and a decrease of luminescence intensity should be observed.

In the following table the ratio of the intensities of the vibronic modes for the luminescence (upright fonts) and the excitation (italic fonts) spectra are compared:

	T	D+T	2T
D	1.08 *1.06*	11.7 *6.68*	33.1 *18.2*
T		10.8 *6.32*	30.6 *17.2*
D+T			2.83 *2.78*

The ratio of the intensities are comparable and within the uncertainty of the measurements. Unfortunately, the highest vibronic mode in energy which

was clearly detectable is less than 600 meV above the zero phonon peak, where the band edge is expected.

4.5 Additional Peak when Exciting around 2.54 eV

4.5.1 Characterisation of the Spectra

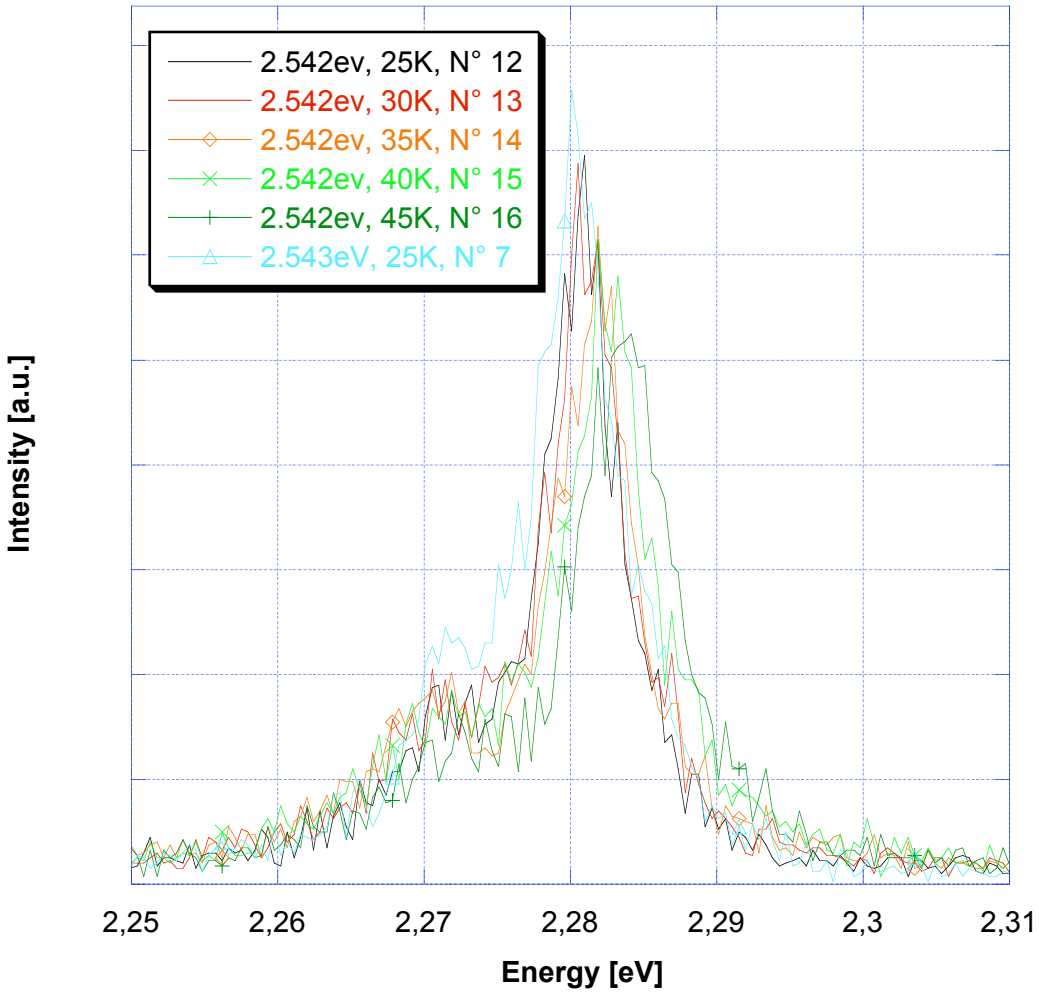

Figure 19: Spectra around the zero phonon line for different excitation energies around 2.54 eV. For an interval of about 4 meV, an additional peak appears at lower energy than the zero phonon line, near 2.27 eV.

For excitation energies between 2.537 and 2.546 eV a second peak appears in the luminescence spectrum at an energy of about 8.5 meV below the zero phonon line (cf. figure 19). This behaviour was found on sites with visibly

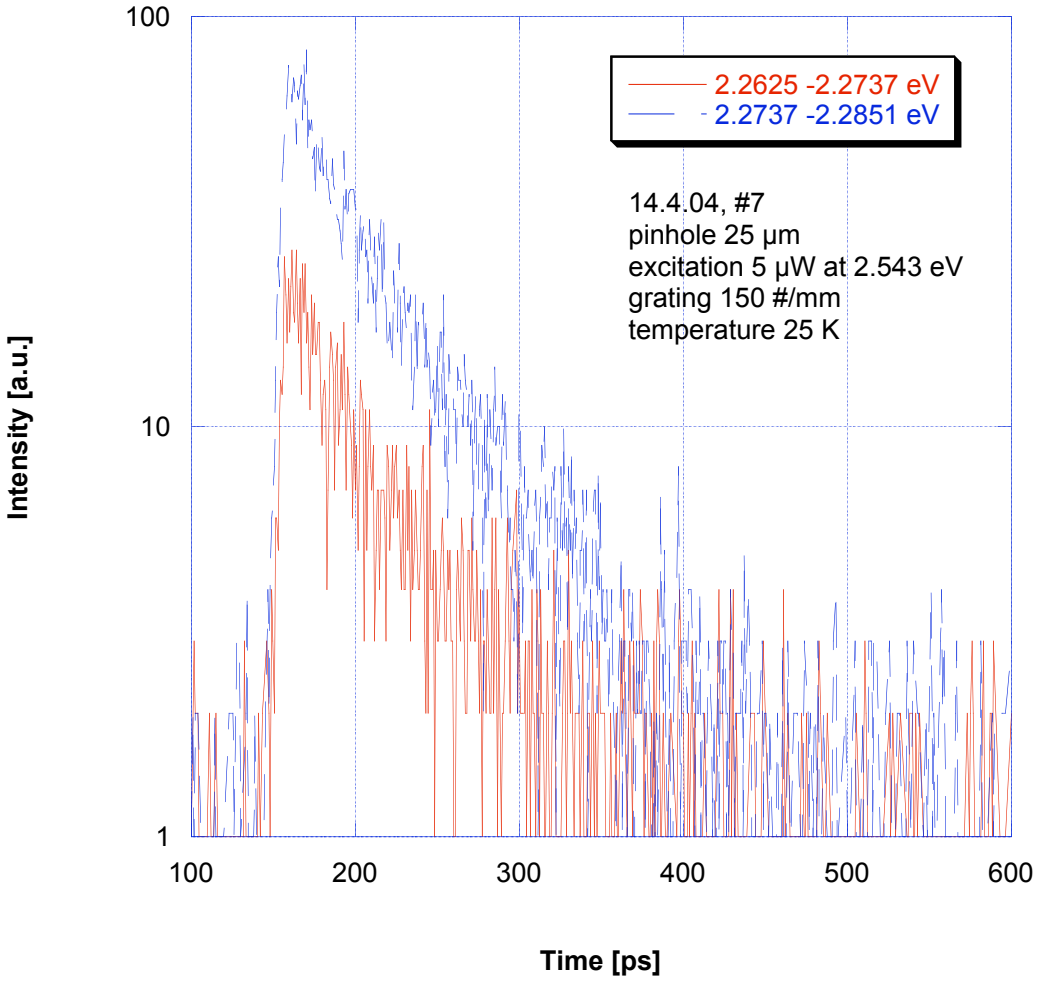

Figure 20: Luminescence signal of the two peaks of spectrum number 7 in figure 19. The more intense signal is from the peak which is always visible, independent of the excitation energy. The recombination times of the two signals are identical.

intenser luminescence, situated about 1-2 mm on the border of the sample. The two signal have the same lifetime and this time does not differ to those estimated for other excitation energies, in particular the times become shorter for lower temperatures. The ratio of the two peaks seem to be dependent of the excitation energy, but equal for different temperatures for the same excitation conditions. This second peak has been detected only at these excitation wavelengths. It cannot however be excluded that it may appear in other narrow ranges that were missed because of the low energy resolution of our excitation spectrum.

temperature [K]	excitation energy [eV]	ratio of intensities
15	2.540	0.78
15	2.542	0.79
15	2.544	0.64
25	2.543	0.33
25	2.542	0.43
30	2.542	0.41
35	2.542	0.47
40	2.542	0.45
45	2.542	0.40

The uncertainty on the excitation energy is of 2.6 meV. The last 5 lines on the table are done with identical excitation because the laser remained stable during all the measurements.

When analysing more carefully the absorption around the T line, shown on figure 12(b), one remarks that the lower energy flank is more important than the one on high energies. This cannot be explained by a thermal distribution. Also the composed state, build of an exciton and an optical phonon T, has a dispersion with a positive second derivative in the energy. Therefore the high energy flank would be more important. A fit containing two lorentzian functions gives a good result, as can bee seen on figure 21. Furthermore, the separation between the two peaks is 6.8±2.3 meV, about the energy difference we found in the fluorescence of the zero phonon peak and the additional peak appearing at lower energies. The ratio of intensities are also comparable to those found in the excitation measurement:

11 K	30 K	50 K
0.43	0.57	0.52

The width seems a little larger than for the T line: 6.7±2 meV. The absorption measurements were performed on a different sample than the excitation measurements.

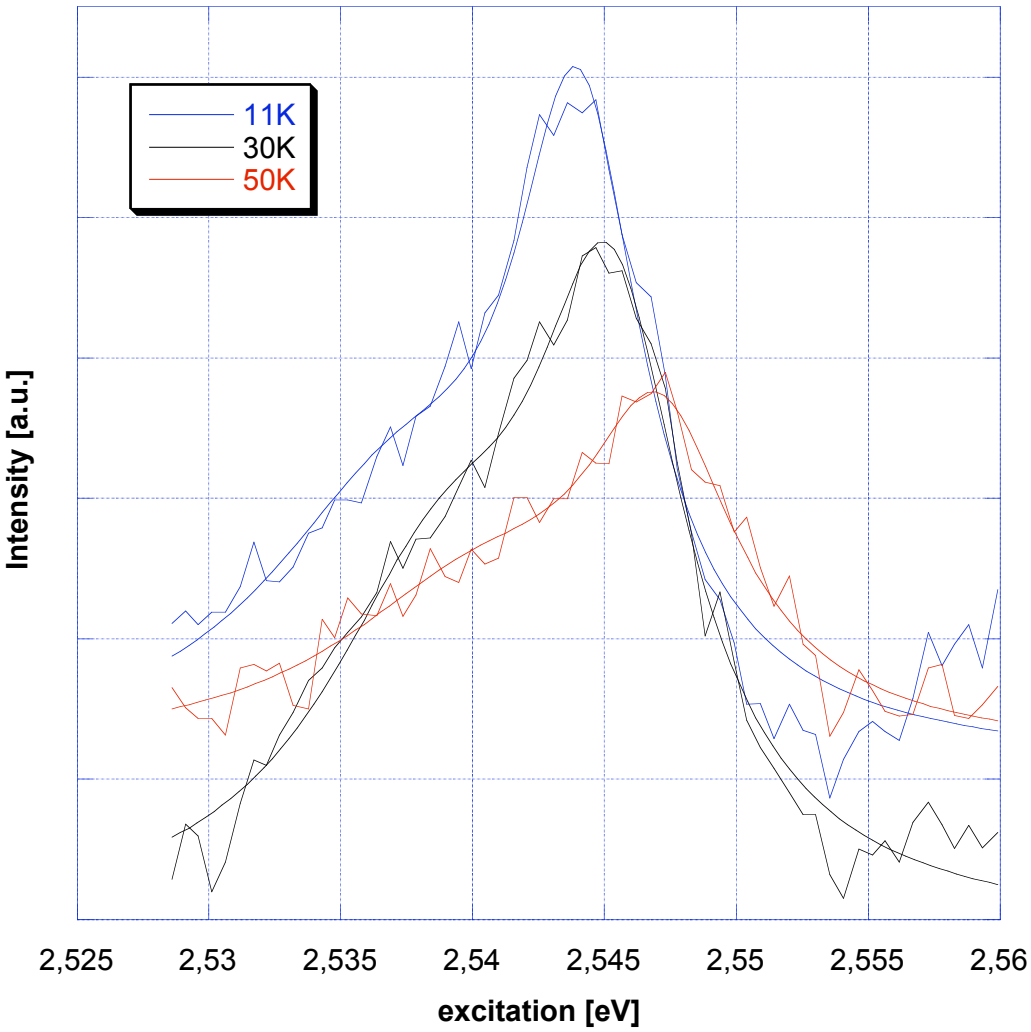

Figure 21: Fit of the T absorption line by two lorentzian functions.

Near the D line, around 180 meV above the zero phonon line, the appearance of a second peak was not observed. There remains still the possibility that we were not able to stabilise the laser at the mode with the necessary excitation energy, considering that the stable modes are separated by about 10 to 20 meV.

4.5.2 Tentative Interpretations

The additional peak in the absorption spectra near the T vibronic line suggests that the situation described in the previous section is independent of the location on the sample.

As the two peaks have the same lifetime, independent of the temperature, the excited states from which the emissions are comming are in equilibrium.

The distance in energy between the two peaks (about 8 meV) is too large to have a direct thermal equilibrium between a hypothetical complex and the zero phonon line (45 K correspond to 3.8 meV).

The same lifetimes independent of the excitation energies and no significant differences in the intensities indicate that there is no additional channel which becomes active.

We exclude the possibility that the band edge is located at this energy. All other indications locate the gap at an energy higher than 500 meV above the zero phonon line. But, more important, if the effect with the two peaks would be an indication of the continuum spectrum, it should be visible over a much larger interval of excitation energies above the threshold.

A possible explanation could be that we have a band crossing. This would explain the narrowness of the excitation zone. The problem with this interpretation is that an additional channel would be opened. But the experimental data indicate no such channel.

Clearly additional data are needed. The experimental setup would need a resolution of about 1 meV in the excitation. It would be interesting to verify if the double peak is systematicaly found everywhere on the sample with the same intensity related to the usual one.

Other interesting measurements would be to verify if the effect remains if the sample is heated above 100 K, where the thermal energy becomes more important than the separation. We have verified that the additional peak is not visible near the zero phonon line in absorption spectrum, but were unable to check this for the D line. It would also be interesting to excite near the D line or at two times the energy (around 2.80 eV).

4.6 Conclusion

With the help of the excitation measurements, we were able to locate the vibronic modes of the carbon bonds of the polymer backbone. The differences in energies for the vibronic modes between the fluorescence and excitation spectra were found to be very small. Also the ratio of one vibration mode to a multiple of this mode is comparable for the fluorescence and excitaion spectra. With the resolution in the excitation and the accuracy of the luminescence intensity of our setup, we found no evidence of the band edge.

To locate the band edge on the red chain, a setup with a much better resolution in the excitation has to be used. CW measurements would also give a more precise spectra regarding the intensities.

With a setup having its excitation modes separated by about 1 meV, one would also be able to clarify the additional peak near the zero phonon line appearing only for a very small excitation interval.

5 Radiative Lifetimes at Low Temperatures

5.1 Introduction

This chapter deals with the evolution of the exciton radiative lifetime in function of the temperature. Theoretical models show that the radiative lifetime is a function of the temperature and depends on the dimensionality of the structure [And91, Cit92, Cit93]. Specifically for one dimensional systems the lifetime is proportional to $\sqrt{T}$. This leads to the question what happens at very low temperatures. For other quantum wires, the square root law is valid only for a small domain from 30 to 70 K. At lower temperatures fluctuations in the lateral confinement potential lead to localisation [Obe00]. 3BCMU follows the square root law for a temperature down to 10 K [Lec02]. The aim of the present experiments was to extend the temperature range down to a region where the $\sqrt{T}$ law breaks down because of residual disorder.

5.2 Technique

The measurements in this chapter were performed with the setup described in section 3, using a liquid helium bath cryostat. The sample was excited at the energy of the T vibronic line of the red phase. We obtain images with information about the spectral and temporal aspects of the luminescence of our samples.

Suppose we have a two level system with a radiative and a non radiative channel. The intensity of the luminescence depends on the number of particles in the excited state. This leads to the following rate equation:

$$\frac{dn}{dt} = -n/\tau_{eff}$$

The lifetime of this state is called the effective lifetime and its inverse is the sum of all inverse lifetimes which are involved. There is namely the radiative lifetime, in which we are interested in this work, and several possible non radiative lifetimes from channels as for example recombination by impurity sites, band crossings and fission or non radiative decay to a lower lying state.

The radiative lifetime is found to be dependent on the temperature and this function is characteristic of the dimensionality of the structure observed. For quantum wires the lifetime is proportional to the square root of the temperature, for quantum wells, it is linear. A more detailed discussion of the origin is given in section 5.3 on page 45

Previous measurements on the red chains showed this behaviour of the radiative lifetime over a temperature range from 10 to 100 K [Lec02]. Furthermore it was shown that the non radiative lifetime is constant up to 50 K

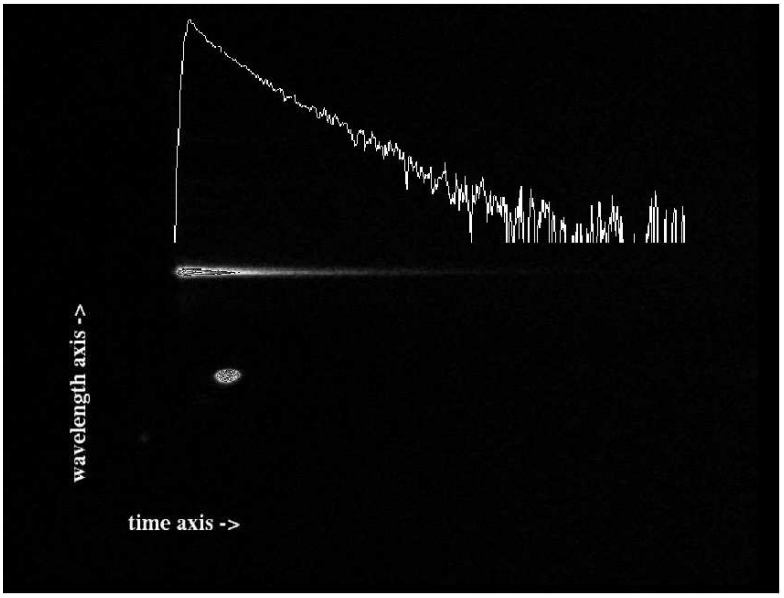

Figure 22: Typical luminescence spectrum at 15 K. The vertical axis reports the wavelength, the horizontal the time. The profile at the top shows the temporal response of the zero phonon line with a logarithmic intensity axis. The bright spot on the lower left part is the laser (for further details on the setup, cf. chapter 3).

and decreases exponentially for higher temperatures because of non radiative channels becoming active.

The absolute intensity measurements necessary to determine the quantum yield are delicate because of the following two points: First, the absorption coefficient of every sample is different, inhomogeneous and evolves with every phase change at 120 K. Second, to collect all the emitted light is not an easy task.

There are three possible ways to verify the square root law. For two of them the radiative lifetime is estimated and compared to the square root law. For the third method, a resolution in time is not necessary.

- We can measure the effective lifetime by measuring the luminescence intensity in function of time and the quantum yield. As the quantum yield is given by
$$\eta = \frac{\tau_{eff}}{\tau_{rad}}$$
the radiative lifetime can directly be extracted. The quantum yield is equal to the ratio of the luminescence intensity to the absorbed energy

of the laser pulse over one cycle, which is also equal to the ratio of the transition probability of the radiative channel to the transition probability of the relaxation, radiative and non radiative channels combined. The relation above is a direct consequence of the equality between the transition probability per unit of time and the inverse of the lifetime.

- The second method is to estimate the initial intensity I_0 of the luminescence signal. The total luminescence intensity I is given by

$$I = I_0 \int_{\text{lumin. decay}} \exp\left(-\frac{t}{\tau_{eff}}\right) dt \approx I_0 \tau_{eff}$$

  Furthermore, A being the absorbed energy:

$$\eta = \frac{\tau_{eff}}{\tau_{rad}} = \frac{I}{A} = \frac{I_0 \tau_{eff}}{A}$$

  The radiative lifetime is proportional to the inverse of the initial luminescence intensity if the absorption is maintained constant, which means a constant incident photon flux *and* a constant number of absorbing chains. The latter implies a strict constancy of the laser spot on the crystal (better than 10 μm).

- The last method is to observe the relative intensities between the zero phonon (ν_0) emission I_0 and some phonon line, typically I_D, the intensity of the double carbon bond vibronic line of the polymer backbone (ν_D). The ratio I_D/I_0 is depending on the dimensionality of the observed structure. In our case, for a 1D structure, we have

$$\frac{I_D}{I_0} \propto \sqrt{T}$$

We did not use the second method because the error of the initial intensity was too large. The initial intensity is extremely dependent on the stability of the laser pulse. A fluctuation in either width, intensity or a temporal drift have an important impact on the initial intensity. Additionally, the problem of spatial stability of the sample is present.

The last method has the advantage that we don't have to estimate a lifetime. The temporal stability of the setup is not crucial because the total intensities of the lines over the period of a pulse are compared. Fluctuations of the laser introduce an error of the same amount on the two lines. The drawback is that the intensities of the two lines differ by two orders of magnitudes. To compare the intensity of the zero phonon line with a vibronic

line (D or T), we need at least 3 order of magnitudes in the intensity, which leads to an integration time of about 20 min. Even the spatial stability on the sample is not important, as long as the different sites have an emission which follows the square root law. In such an inhomogeneous situation the proportionnality constant between the ratio of the intensity and $\sqrt{T}$ would be meaningless. Also the sensitivity of the detection can be different at the two regions of different wavelengths. The derivation of this law is given below in section 5.3.1.

In the first method the integration time is much shorter at around 3-5 min because only the signal of the zero phonon line is measured. The importance of the spatial stability mention above remain and the excitation has also to remain stable at least during a measurement. But the most problematic point is the estimation of the quantum yield. These results to suppose the non radiative lifetime to be constant at temperatures below 50 K.

The linear response of the streak camera is crucial. If the intensity response is non linear, an exponential decay is not seen as mono exponential anymore. We performed tests where we changed the intensity of the signal and put attenuators in front of the camera. The intensity detected follows the ratio (excitation energy):(attenuation) with an error of about 20%. The fluctuation in the temporal response is caused by the stability of the laser and the synchronisation of the streak camera.

5.3 Theoretical Background

5.3.1 Ratio of Intensities of the Zero Phonon and D Lines

In the following section the dependence of the ration of the intensities of one of the vibronic lines to the zero phonon line is explained. For the zero phonon line, only states complying $k < k_0$ contribute to the luminescence because of the conservation of the component of momentum parallel to the chain, where k_0 is the wavevector of the emitted photons. Whereas for the recombination to a state formed by one of the vibronic lines, the vibration being an optic phonon, states of all k are allowed to recombine, the created phonon taking care of momentum conservation. As we suppose that the probability of recombination for the different states to D is constant[‡] the ratio of the intensities is proportional to $\zeta(T)$, the ratio of the states participating to the respective recombinations. By assuming a Maxwell-Boltzmann distribution

[‡]The recombination times could also vary slightly without invalidating the analysis, since we take a mean value of the probabilities of all the different k states participating in the recombination, and since at the low temperature used, only exciton k states close to the centre of the Brillouin zone are involved, and this centre is not a singular point.

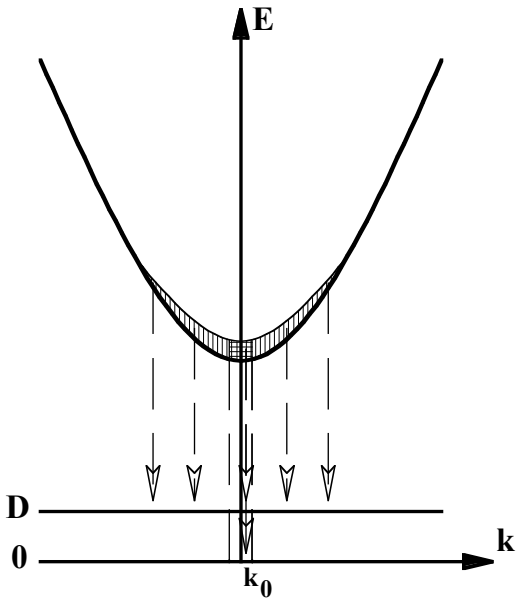

Figure 23: Scheme showing the excited states participation to the recombination to the ground states (dashed horizontally) and to the state formed by an optical phonon D (dashed vertically). Only states with $k < k_0$ contribute to the recombination to the ground state.

for the excitons, $\zeta(T)$ is given by

$$\zeta(T) = \frac{\int_0^\infty D(E)\exp(-\frac{E}{k_BT})dE}{\int_0^\Delta D(E)\exp(-\frac{E}{k_BT})dE} \tag{4}$$

where $D(E)$ denotes the density of states of the excitons ($\propto 1/\sqrt{E}$ for 1D) and $\Delta = \hbar^2 k_0^2/2m_{ex}$ the maximum kinetic energy of excitons which can decay radiatively to the ground state. This gives:

$$\zeta(T) = \frac{\sqrt{\pi k_B T}}{\sqrt{\pi k_B T}\,\mathrm{erf}(\sqrt{\frac{\Delta}{k_BT}})}$$

Assuming $T \gg \Delta/k_B \approx 1$ K and linearising $\mathrm{erf(x)} = 2/\sqrt{\pi}\int_0^x e^{-x^2}dx = 2x/\sqrt{\pi} + O[x]^3$:

$$\frac{I_{D,T}}{I_0} = \zeta(T) \approx \sqrt{\frac{\pi k_B T}{4\Delta}} \propto \sqrt{T}$$

Going to very low temperatures, we expect at some value that the radiative lifetime will cease to follow the square root of the temperature. The

conservation of the wavevector during the relaxation of the excitons fixes the energy of the excitons which emit a photon of the energy of the zero phonon line at 68 μW. This corresponds to a temperature of 0.8 K. At least near this temperature we expect the radiative lifetime to become longer than predicted by the square root law. Excitons with lower energy would need to interact with phonons to justify the conservation of the wavevector. The concentrations on phonons being proportional to the temperature of the monomer matrix, the interaction becomes less and less probable as the temperature falls. A deviation to the square root law can occur at a temperature higher than mentioned above, if fluctuations in the confinement are large enough.

At high temperature the square root law becomes invalid because optical phonons become thermally accessible or the thermal energy becomes comparable to the binding energy of the excitons, which leads to a coexistence of free carriers and excitons. This is the case in V-groove AlGaAs/GaAs quantum wires for temperatures above 60 K [Obe00]. As the binding energy of the exciton of the red chain is expected to be much larger (around 580 meV compared to 11 meV), the radiative lifetime will continue to be valid at higher temperatures. At temperatures over 50 K a non radiative channels becomes efficient and will dominate the recombination for higher temperatures such that the quantum yield will become too small leading to a signal too weak to determine the radiative lifetime.

5.3.2 Dependence of the Radiative Lifetime on the Temperature

The radiative lifetime or its inverse, the radiative recombination rate is proportional to the number of states contributing to the radiation divided by the total number of excitonic states which are thermaly accessible. The states contributing to the radiation are those with $\|\mathbf{k}\| \leq \|\mathbf{k_0}\|$. The ratio of the contributing to the total state is identical to equation (4). This gives for the relaxation rate

$$\zeta(T) \propto \sqrt{\frac{4\Delta}{\pi k_B T}}$$

for the one dimensional case and

$$\zeta(T) \propto \frac{\Delta}{k_B T}$$

for the two dimensional case. The radiative lifetime for a one dimensional system is thus

$$\tau_{rad} = \tilde{\tau}_{rad}\sqrt{T}$$

[Cit92] gives an expression of the radiative lifetime, which is

$$\tau_{rad} = \frac{2m^*_{ex}m_0c_0}{2\alpha E^0_{ex}}\frac{1}{f_L}\sqrt{\frac{k_BT}{\pi E_1}}$$

where $\alpha = 1/137$ is the fine structure constant, E^0_{ex}=2.28 eV is the exciton energy at $\mathbf{k} = 0$, $E_1 = \frac{(\hbar\mathbf{k})}{2m^*_{ex}m_0}$ is the energy of the exciton with the same wavevector as the emitted photon and m^*_{ex} the exciton effective mass. f_L is the exciton absorption oscillator strength per unit length of the chain. f_L was estimated for the blue chain and has a value of $f_L = 6 \cdot 10^8 m^{-1}$. Assuming that f_L is similar for the red chain, the law found for the radiative lifetime in [Lec02] of $\tau_{rad} = (80 \pm 20)\sqrt{T}$ ps/$\sqrt{\text{K}}$ gives an effective exciton mass of $m^*_{ex} = 0.3 \pm 0.1$. This value seems reasonable, since the reduced carrier mass of the blue chains, as measured by electroabsorption, is slightly less than 0.1 [Hor96].

The calculations of the ratio of the intensities in the previous chapter and the radiative lifetime are done under two assumptions:

1. The excitons are free, they are not bound to impurities.

2. $\mathbf{k_z}$, the wavevector along the polymer chain is conserved.

A rapid thermalisation of the excitons is achieved by interaction with logitudinal accoustic phonons of the monomer crystal [Dub04].

Contary to epitaxial grown semiconductor structures, as for example AlGaAs/GaAs compounds, the polymer chains show no interface fluctuations. Fluctuations in these compounds come from the variation of the thickness of the structures which are difficult to control during growth. The lateral confinement in the chain is controlled by the covalent binding between the carbon atoms of the polymer backbone. The confinement potential can thus only be influenced by inmpurities or defects in the monomer matrix.

5.4 Presentation and Discussion of Low Temperature Measurements

In this section we present the measurements of the effective lifetimes at temperatures between 2 and 10 K. An overview of the measurement series performed on different locations on the sample are presented in figure 24. For certain series we are able to extend the square root law to temperatures down to 2 K. Those results are presented in the following section. For other series the radiative lifetime does not follow the square root anymore. The results of these series and explanations for the deviation to the law are presented in the second next section (5.4.2).

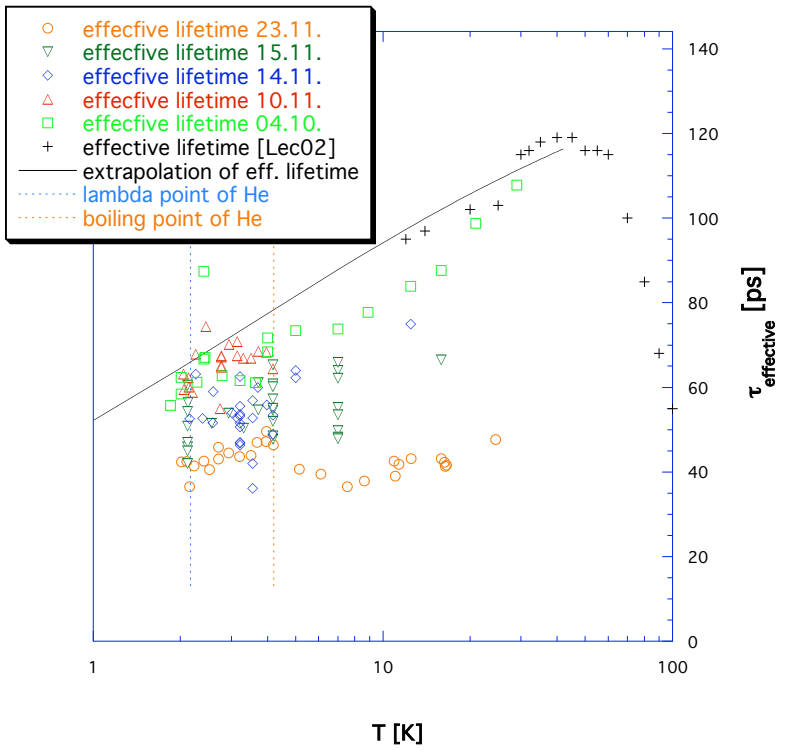

Figure 24: Overview of the effective lifetime of the different series. The series are from measurements on different locations on the same sample and were taken on different days (date given in legend). The continuous line shows the extrapolation to lower temperatures of the square root law published in [Lec02]. The different series are discussed in the sections 5.4.1 and 5.4.2.

5.4.1 Radiative Lifetime at Low Temperatures $\propto \sqrt{T}$

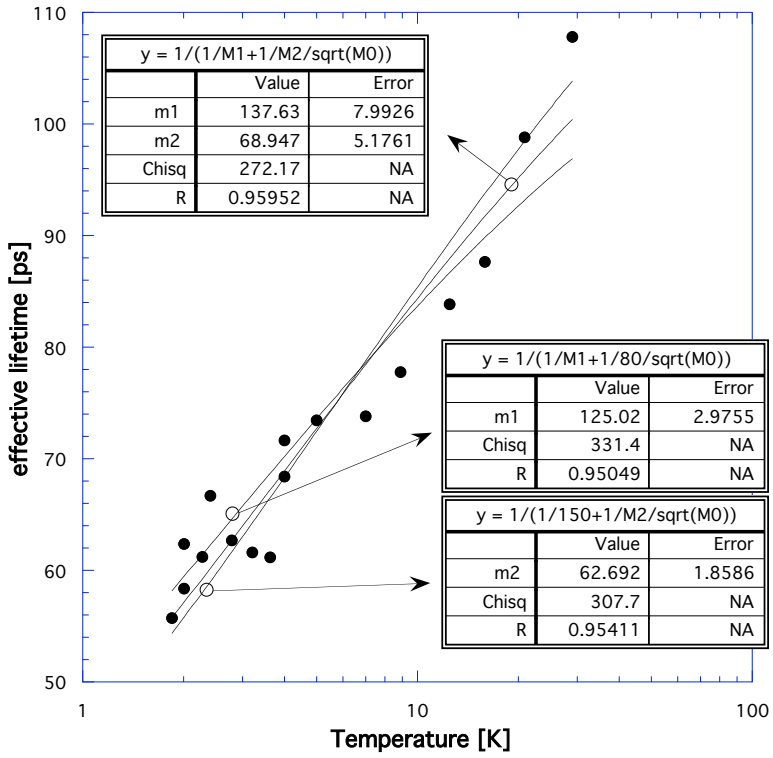

Figure 25: This figure shows the effective lifetime in function of the temperature. This series of measurements was taken on a fresh sample. The fits were done under the assumption of a constant non radiative lifetime and a proportionality between the radiative lifetime and the square root of the temperature. In two of the fits, one of the parameters was fixed at the mean value given in [Lec02]. In the third, the two parameters were left free.

Figure 25 shows that the radiative lifetime is proportional to the square root of the temperature if a constant non radiative lifetime is assumed. This is reasonable since the opening of a new channel below say 4 K would imply a threshold about 200 μeV above the k=0 state of the exciton, a quite unlikely situation. The fit on the figure give a non radiative lifetime of 140±10 ps and a proportionality factor of 70±7 ps/$\sqrt{K}$. These results are in agreement with the values published in [Lec02]: τ_{nr}=150±15 ps and τ_r=(80±20)$\sqrt{T}$ ps.

The ratio of the intensity of the vibronic modes to the zero phonon line is reported on figure 26. This measurement is not dependent on a stable excitation. The fit with an additional constant is clearly better. The constant describes the noise on the measurement. The constant of around 0.003 would

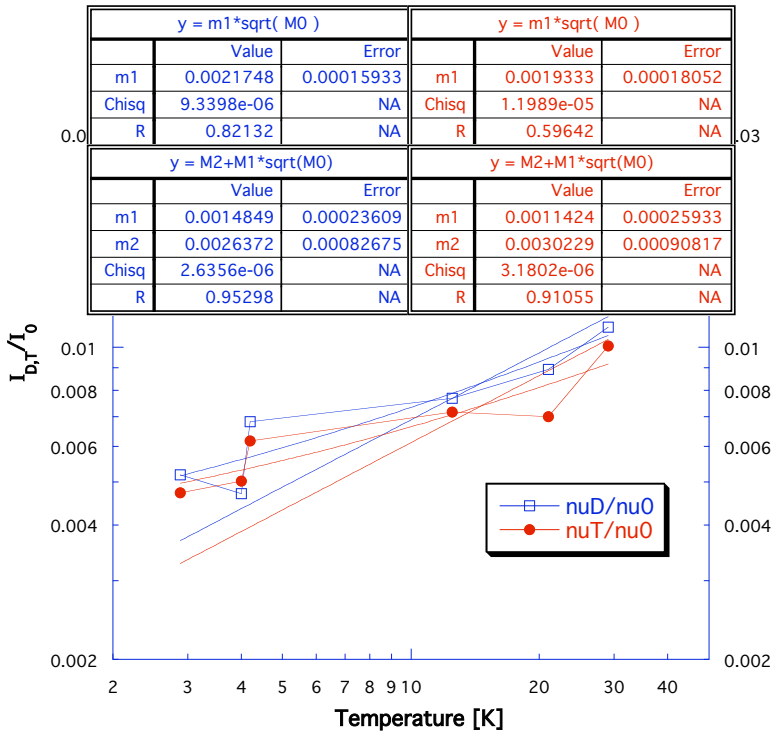

Figure 26: Figure showing the ratio of the integrated intensity of the vibronic mode D (resp. T) to the intensity of the zero phonon line. The points are fitted by a square root law and the same law with an additional constant for the noise, which affects the $I_{D,T}$ value more.

suggest that the background on the spectrum at the energies of the zero phonon and the D line differs by around 2/3 counts. This is a quite reasonable amount of the variation of the noise from one region to the other of the streak camera.

5.4.2 Deviation to $\sqrt{T}$

Description of the Deviation to $\sqrt{T}$ Several series on the same sample do not fit with the results of the previous section. Typically the spreading of the measured values becomes important. For some series, the effective lifetime seems to saturate at lower temperatures. A representative example is given in figure 28. A fit supposing a constant non radiative lifetime results in a shorter non radiative lifetime and a larger prefactor $\tilde{\tau}_{rad}$ for the square root law of the radiative lifetime. Typically the effective lifetime saturates at temperatures below 10 K. On certain decays we observed a non exponential

decay. In general the series tend to have shorter lifetimes than those reported previously in [Lec02] (see figure 24). We also observe a more important fluctuation in the intensities of the luminescence, probably corresponding to stronger local variations of chain density and radiative lifetimes. We present here the differences to the measurements in the previous section.

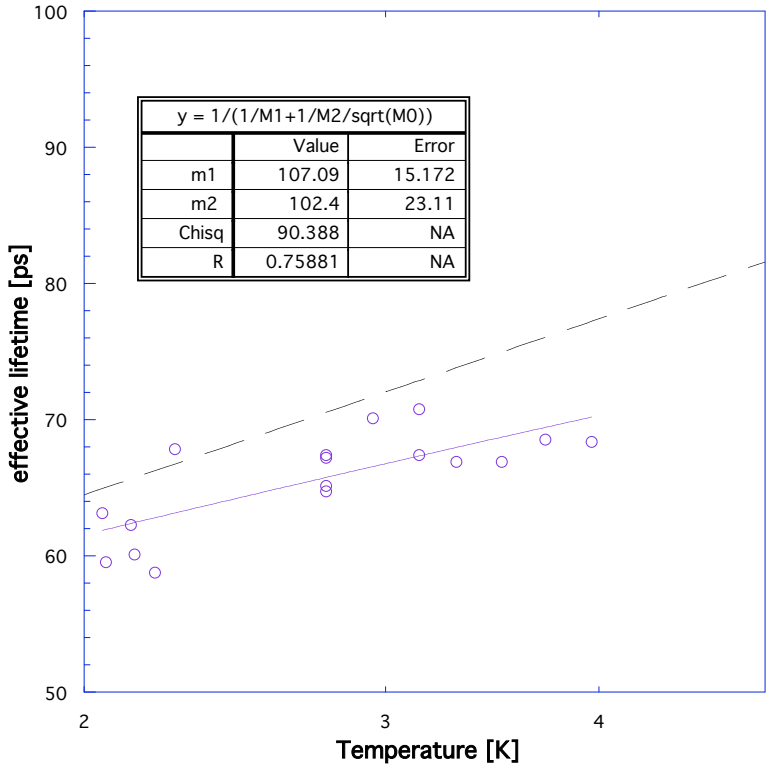

Figure 27: The effective lifetime in function of the temperature. The dashed line shows the effective lifetime as published in [Lec02] extrapolated to the temperatures shown on the x axis.

In figure 26, it is also visible that the ratio I_D/I_T is not always constant. For the measurements at 20 K, the intensity of the T line seems abnormally weak, for the temperature of 4 K it is the D line. This is unexplained, but might be an instrumental effect, since the sensitivity pf the streak camera decreases near the top of the screen, and this effect may not have been well taken into account.

Explanations of the Deviation to $\sqrt{T}$ Before discussing the possible physical or technical reasons for these different results, I want to stress the fact that these measurements are done with measurement errors becoming

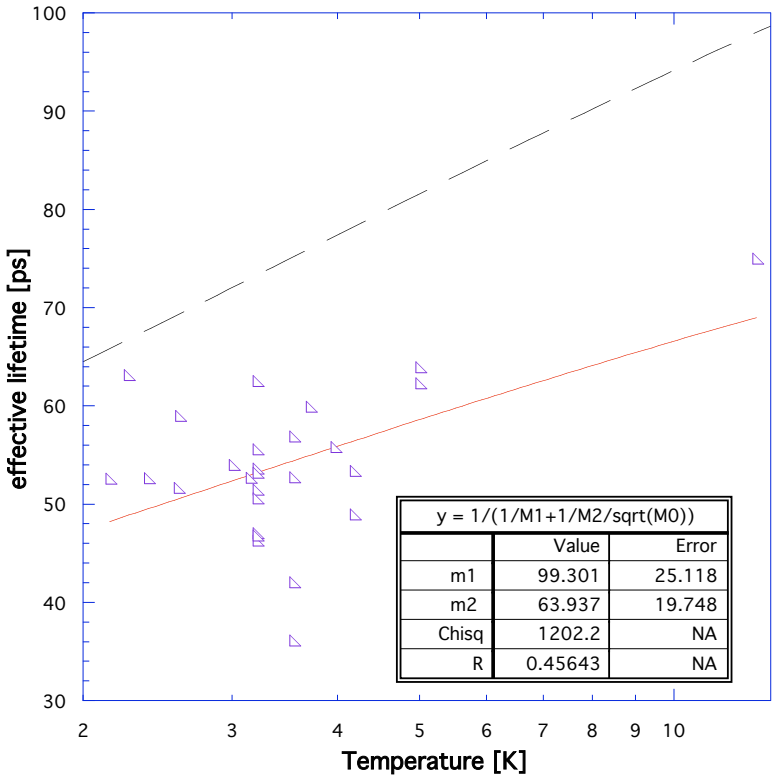

Figure 28: The effective lifetime in function of the temperature. The dashed straight line shows the effective lifetime as would be expected. At temperatures below 3 K, the lifetime seems to saturate.

important at low temperatures. At temperatures above 10 K, the radiative and non radiative lifetimes were estimated at $80\pm20\sqrt{T}$ psK$^{-1/2}$ and 150±15 ps [Lec02]. For example an error of 0.5 K on the temperature, which is quite reasonable, leads to an uncertainty of about 6 ps in the value of the radiative lifetime at 10 K ($\Delta\tau_{rad} = \tilde{\tau}_r/(2\sqrt{T})\Delta T$, where $\tau_r = \tilde{\tau}_r\sqrt{T}$). At lower temperatures this error is more important. For 2 K an error of 14 ps has to be considered.

In figure 29 the effective lifetimes at 3 different temperatures are reported for different positions of the sample. In the following table we present the relative error for the 3 temperatures:

temperature [K]	eff. lifetime [ps]	error eff. lifetime	relative error
2.12	51.35	9.33	0.182
4.18	56.49	8.82	0.156
7.00	56.90	8.96	0.157

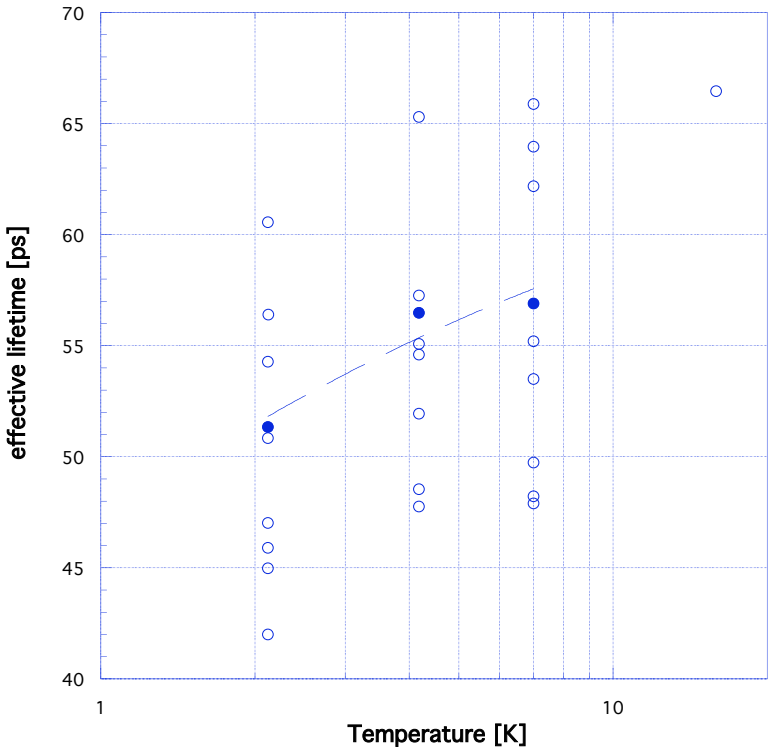

Figure 29: The effective lifetime in dependence of the position of the excitation spot on the sample for 3 different temperatures (2.12 K, 4.18 K, 7 K). The 3 solid dots are the lifetimes centred between the two extremal times.

The effective lifetime was taken as the mean value of the two extreme times and the error is the difference of this value to to extreme value.

The extraction of the decay time is not trivial. Depending on the background subtracted and the fitting interval chosen, variation of up to 15% are observed.

Explanation by exciton localisation on the chains In general we observed a tendency that the deviation to the situation presented in the previous section becomes more important with time. This is an indication that the samples "ages". A broadening of the luminescence lines is observed after several heating and cooling cycles. The excitation beam creates initiation sites for future polymerisation, which happens when heating the sample above 170 K. At 150 K is a phase transition in the crystalline structure of the monomer. During this transition the angle β varies slightly. Planes in which the polymers are placed slide one in respect to the other at the transition, and if the process is not fully reversible dislocations and stocking faults are

created: Heating and cooling across this temperature will induce faults in the monomer matrix. Also a higher concentration in polymers increases the interaction between the chains. More important than the electronic interaction, which has a rather short range of about 1 nm, is the influence of faults to the potential of a polymer. All this results in a fluctuation of the confinement potential along the chain leading to localisation at low temperatures. If the thermal energy of the excitons is in the range of the fluctuations the excitons are localised. The model of a one dimensional structure is not accurate anymore. The chain is better described by a succession of quantum dots. We think that the series presented in figure 30 represents the case, where the chain has to be seen as a succession of quantum dots. Indeed it was measured on a sample which has aged. The measurements were performed on the same sample as the series showing the square root law (cf. figure 25), but 45 days later. The lifetime of an exciton confined in a quantum dot, where the energy separation between the ground state and the first higher exciton state is larger than k_BT, is almost independent of the temperature [Got97, Oku98]. This is a direct result of the δ-functionlike density of states of the excitons confined in dots. Microphotoluminescence measurements show that the luminescence extend over length of chains of up to 30 μm [Dub04]. On some chains the emission seems to be cut in two separated regions as shown in figure 31 [Dub04], and this is in a high quality fresh monomer crystal.

The presence of an infinite long polymer does not induce a fluctuation into the potential. But the ends of the polymers act as point defects generating an elastic stress field. The intensity of deformation goes at r^2, and as the probability of the presence of polymers is also r^{-2}, they compensate each other, the order of potential fluctuations should be homogeneous and only dependant of the degree of polymerisation of the sample.

The initiation sites of polymerisation are irrelevant as faults, since they are of molecular size [Six84]. The intensity of the fault rises with the length of the polymer.

Instrumental effects affecting the determination of τ_{rad} at low T
Most of the excitation energy is absorbed by the blue chains and does mainly heat the sample. Figure 4 gives an indication of the ratio between the absorbed energy of the red and blue chain. The optical density of the blue phase at the T vibronic line is typically 0.05 for the blue phase and about $2{\cdot}10^{-4}$ for the red phase, hence the red chains contribute only about $4{\cdot}10^{-3}$ to the absorbed energy. As the specific heat coefficient depends on the temperature (T^{-3}), the sample is more heated at lower temperatures, supposing the excitation intensity constant for all measurements. In appendix A an es-

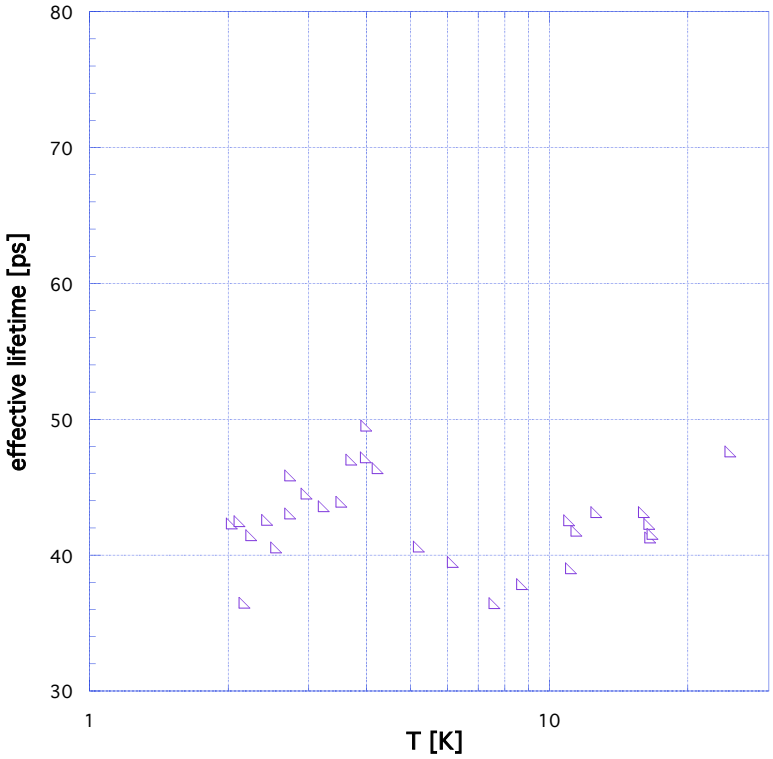

Figure 30: Series of measurements where the effective lifetime remains constant over the temperature range of 2 to 25 K. This is a typical characteristic of the lifetime of excitons confined in a zero dimension structure.

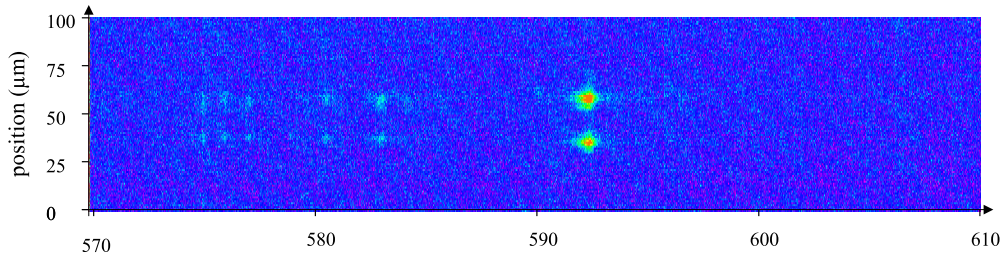

Figure 31: Image showing the luminescence of the D vibronic line. On the y axis is the spatial dimension along the polymer chain. On this image, the luminescence is splited in two sites of about 10 μm, whereas normally the luminescence is sometimes seen over an extension of up to 30 μm [Dub04].

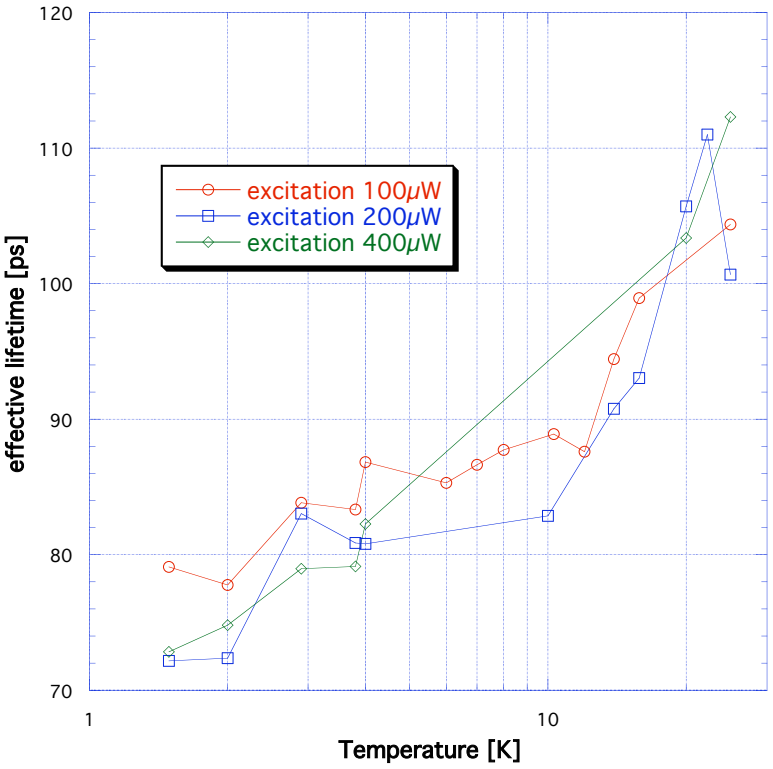

Figure 32: The effective lifetime in function of the temperature for three different excitation intensities.

timation of the temperature distribution across the sample is done. Instead of an exponential decay, the signal has a more complex form. The radiative lifetime will be overestimated for the nominal temperature. This effect will depend on the excitation energy and the temperature of the helium bath. The estimation in appendix A shows that for temperatures over 3.5 K and excitations of only some hundreds of μWatts, the difference in the decay is in the order of less than some hundredths of the intensity. Figure 32 shows that a variation in the lifetime for different excitation energies is not detectable. These measurements were performed on a different sample than the one on which the series presented in this chapter were obtained from. The chains were excited by the D vibration line, but this should not lead to any difference compared to the measurements excited by the T line (cf. page 24).

At the interface between the sample and the helium bath, the heat exchange does also depend on the temperature and the materials involved (Kapitza [Bat00, Pol69]). There is a lot of information available about the Kapitza effect for an interface with metals [Pol69], but for polymers or organic materials little is known. As the resistance manifests itself as a factor

proportional to T^{-2} in the thermal distribution, the difference in temperature of the centre of the sample to the helium bath can become quite important at lower temperatures. In some cases a cooling of the sample can effectively heat the centre of the sample. In the 1D case, this will result in a distribution of radiative lifetimes, the one in the centre being larger than the one on the surface.

As mentioned before (p. 52), for some decays we observed a non-exponential form. Fitting with a function of the form $\exp(-(t/\tau_{eff})^{\beta})$ gives better results. The interpretation of β is not obvious. It could describe a distribution of emitting sites with similar radiation times, perhaps resulting from temperature non uniformity. We observed that the quantity τ_{eff}/β was constant and proportional to the energy emitted :

$$I \propto \int_0^{\infty} \exp(-(\frac{t}{\tau_{eff}})^{\beta})dt = \frac{\tau_{eff}}{\beta}\Gamma(\frac{1}{\beta})$$

($\Gamma(1/\beta)$ is nearly constant).

The question remains if we are observing an effect with a physical reason or if the non exponentially is due to a non linearity of the sensibility or the temporal response of the streak camera.

Effect of a varying non radiative lifetime Up to now we supposed that the non radiative lifetime remained constant at lower temperatures. We know that this is true for temperatures between 10 and 50 K. Above this temperature a non radiative channel begins to dominate the recombination [Lec99]. We think that this channel is the fission of the exciton of the B_u state in two triplet excitons state, similar to the case of anthracene [Sun70, Bou78]. To obtain the quantum yield and the non radiative lifetime, accurate intensity measurements are needed, which are not possible with our setup. We could imagine a situation where a non radiative channel closes below 3 K. If this is not taken into account, as in the above analysis, it will show up as an increase of τ_{eff} and an apparently shorter τ_{rad} as deduced from τ_{eff}, below 3 K. In any case, we do not observe a rise of the effective lifetime below 3 K. Therefore we conclude that there is no additional channel at low temperatures. The diminution of the effective lifetime at higher than 50 K is also thought to be of same nature. This would contradict the explication done before. Also the rise of the non radiate lifetime should be very marked below 3 K, which is not really the case.

5.5 Conclusion

The measurements presented in this chapter show that the law, which links the radiative lifetime of excitons in one-dimensional systems to the square root of the temperatute, can be extended to temperatures as low as 2 K. However, this property seems to be extremely sensitive on the quality of the chains. Disorder breaks the square root law and leads to an effective lifetime less or even independent of the temperature. With our measurements we are not able to characterise the disorder. Therefore a quantitative analysis, which could probably be performed with microluminescence measurements, was omitted.

Our data give no indication of a non radiative channel which becomes active in the temperature range from 2 to 10 K for the series which follow the square root law. We concukde thus that the non radiative lifetime remains constant to temperatures down to 2 K.

A simple model for the heat diffusion in the sample shows that the effect of heating under our excitation conditions has a negligible effect on the lifetimes.

A Estimation on the Impact of the Thermal Resistance on the Sample Temperature

In this appendix the evolution in temperature in the sample is studied. We show that the temperature does not fall to the initial value between two pulses. In approximating the deposited energy as a continuous source, we calculate the thermal distribution and the effect on the radiative lifetime of an excited region in the sample.

A.1 Heat Diffusion during one Pulse Period

The system studied in this chapter is the sample surrounded by the helium bath. We suppose that the sample holder, on which the sample is fixed is at the same temperature as the helium bath and that they act as an infinite reservoir. In one dimension the excited region is in contact to the bath and the sample holder by its surfaces, in the two other dimensions heat is evacuated in the sample. The energy is deposited by a pulse of the excitation beam. We suppose that all the energy deposited in the sample is transformed to heat. The time needed by the system to reach half the initial temperature is compared to the pulse period.

Of the 200 μW of the intensity of the excitation beam, $(1-0.04)^7 = 0.75$ $E_i = 150\mu$W arrive at the sample after crossing 7 dioptres (crystal, 1 lens, 2 windows). The energy deposited by one laser pulse at a repetition rate of 80 MHz is about $2{\cdot}10^{-12}$J. Knowing the optical density (0.05$\pm$0.01 at 2.55 eV) of a sample, its thickness (l=69μm) and the polymerisation rate ($x_p = 5.5 \cdot 10^{-4}$), the absorption coefficient of a fully polymerised sample would be

$$\alpha_p \approx 1.3 \cdot 10^4 \text{ cm}^{-1}$$

The absorbed energy of one laser pulse in the sample with the characteristics described above, would be

$$E_{abs} = E_i \alpha_p x_p l \approx 1.5 \pm 0.5 x_p l$$

The rise in temperature corresponds to

$$\Delta T = \frac{E_{abs}}{\rho V C_p(T)}$$

where C_p is the specific heat, V the excited volume, which is equal to $2\pi l R^2$, 2R the diameter of the spot on the sample of 200 μm and ρ the

A Estimation on the Impact of the Thermal Resistance on the Sample Temperature

density, which is equal to 1.21 g cm^{-3} at 90 K[Lec00]. The specific heat is unknown for 3BCMU, but a comparable polydiacetylene, pTS, has a specific heat of[Eng80]:

$$C_p(T) \approx 3.5 \cdot 10^{-5} T^3 \ (J/gK)$$

This is a typical value for such molecular materials. The rise in temperature is thus at 4 K about 1 mK. We see, the rise in temperature due to a single laser pulse is negligible.

The relaxation in temperature is described by thermal diffusion.

$$\frac{\partial T}{\partial t} = D \frac{\partial^2 T}{\partial x^2}$$

where $D = K/C_p\rho$, with K the thermal conductivity. K is taken as 10^{-4}T (W/cmK), as found for pTS[Mor86]. This is in the same order of magnitude as K=$2.5 \cdot 10^{-2}$W/cmK for a totally polymerised sample of 4BCMU at 300 K, measured orthogonal to the layers formed by the lateral groups[Que93].

We separate the problem in two different situations, one where the evacuation of heat happens through the interface of the sample to the bath, and the other in the two directions into the sample, out of the excited region. We will see, that one of the two processes dominates the other and can thus be taken as an upper limit on the time it takes to cool the sample.

First, we treat the case, where the heat diffuses laterally in the sample. For a infinitely long cylinder with a diameter of 2R, the problem is solved in [Car59, p. 56, eq. (9)] [§]:

$$T = T_i/4 \left\{ \mathrm{erf}\left(\frac{R-x}{2\sqrt{Dt}}\right) + \mathrm{erf}\left(\frac{R+x}{2\sqrt{Dt}}\right) \right\} \left\{ \mathrm{erf}\left(\frac{R-y}{2\sqrt{Dt}}\right) + \mathrm{erf}\left(\frac{R+y}{2\sqrt{Dt}}\right) \right\}$$

A numerical estimation has been done in [Car59, p. 55, fig. 4b] for the time $\tau_{\shortparallel}$, the time it takes that the temperature has half its initial value.

$$\tau_{\shortparallel} = 0.4(R^2/D)$$

Second, for the evacuation through the interface to the bath, the problem is the same as an infinite slab, initially at temperature T_i with its interfaces at temperature T_0. This problem is solved in [Car59, p. 97, eq. (8&9)] and the average temperature in the slab is[¶]:

[§] $\mathrm{erf}(x) = 2/\sqrt{\pi} \int_0^x \exp(-y^2) dy$

[¶] $\mathrm{ierfc}(x) = \int_x^\infty \left(1 - 2/\sqrt{\pi} \int_0^y \exp(-z^2) dz\right) dy$

$$\bar{T} = T_i\Big[1 - 4\frac{\sqrt{Dt}}{l}\Big\{\frac{1}{\sqrt{\pi}} + 2\sum_{1}^{\infty}(-1)^n \text{ierfc}\left(\frac{nl}{2\sqrt{Dt}}\right)\Big\}\Big]$$

A numerical estimation has been done in [Car59, p. 98, fig. 10a][‖]

$$\tau_\perp \approx 0.3(l^2/4D)$$

Comparing the two times, it seems that the heat evacuation directly to the helium bath is more efficient. The heat conduction was supposed isotropic. In a more detailed approach, the heat conduction is probably more efficient in the direction parallel to the sample surface than orthogonal. This is due to the formation of layers in the monomer crystal, stabilised by the H bonds of the lateral groups (cf. figure 1), which are parallel to the surface. Also the phonon propagation is more efficient in direction of the polymers, which are in the layers, oriented in the same direction. Difference of a factor of about 2 are reported for pTS[Mor86].

Considering that $R^2/D = R^2 C_p \rho / K \approx 0.5$ msec, the relaxation time is longer than the period of the laser pulses. The temperature does not fall near the initial value after one pulse period. A different approach has to be taken to quantify the temperature of the sample.

A.2 Temperature in Equilibrium

The thermal relaxation time estimated in the previous chapter justifies to consider the problem as a situation where the heat is continuously deposited in the excited region. The heat is evacuated by the interface of the slab with the helium bath (and the sample holder). This problem is treated in details in [Car59, p. 130] and the temperature is given by

$$T(x) = \frac{A_0}{2K}(l^2 - x^2)$$

where A_0 is the energy deposited by the intensity W of the laser beam:

$$A_0 = \frac{\alpha_p x_p W}{2\pi K R^2}$$

The maximal temperature difference in relation to the helium bath is in the centre of the sample.

[‖]Note that in [Car59] the thickness of the plate is 2l, contrary to our notation (l), hence the division by 4.

$$T(x=0)^{max} = \frac{\alpha_p x_p W l^2}{4\pi K R^2}$$

For typical values ($x_p = 10^3$, $l = R = 10^{-2}$ cm, $W = 10^{-4}$ watt) and a temperature of 4 K, the maximal difference is $T^{max} = 0.3$ K. This is a superior limit as the lateral diffusion is neglected.

If the resistance of the interface to the heat evacuation is considered, an additional term appears. The flux through the interface depends on the temperature difference and a factor H^{-1} (thermal surface resistance). This gives as additional condition

$$\frac{\partial T}{\partial x} - \frac{H}{K}(T - T_0) = 0$$

The temperature at equilibrium is now as follows[Car59, p. 132, eq. 12]

$$T(x) = \frac{A_0}{2K}(l^2 + \frac{2lK}{H} - x^2)$$

The maximal temperature difference becomes now

$$T^{max}(x=0) = \frac{\alpha_p x_p W l^2}{4\pi K R^2}(1 + \frac{2K}{lH})$$

To minimise the difference in temperature through the sample, a lightly polymerised and thin sample, excited by a laser with a low intensity W, has to be used. The intensity of the luminescence is dependent on $\alpha_p x_p^{red} l W \eta_f(T)$, where x_p^{red} is the concentration of polymers of the red phase and η_f the quantum yield of the fluorescence. Not surprisingly, the best compromise between a most uniform temperature distribution and an efficient luminescence is obtained by a sample with a high concentration of polymers of the red phase compared to the total concentration of polymers (x_p^{red}/x_p).

A.3 Impact on the Radiative Lifetime

The radiative lifetime in 3BCMU is shown to obey the following law[Lec02]

$$\tau_{rad} = 80\sqrt{T} \text{ (ps)}$$

As shown in the previous chapter, the temperature depends on the position in through the sample.

$$\tau_{rad} = 80\sqrt{\frac{A_0}{2K}(l^2 + \frac{2lK}{H} - x^2)}$$

A Estimation on the Impact of the Thermal Resistance on the Sample Temperature

To get the intensity of the whole region, supposing that every point emits at the same intensity, we integrate over the thickness ($2l$) of the sample:

$$I = I_0 \int_{-l}^{l} \exp(-t/\tau_{rad}(x))dx = I_0 \int_{-l}^{l} \exp\Big[-t/\Big(80\sqrt{\frac{A_0}{2K}(l^2 + \frac{2lK}{H} - x^2)}\Big)\Big]dx$$

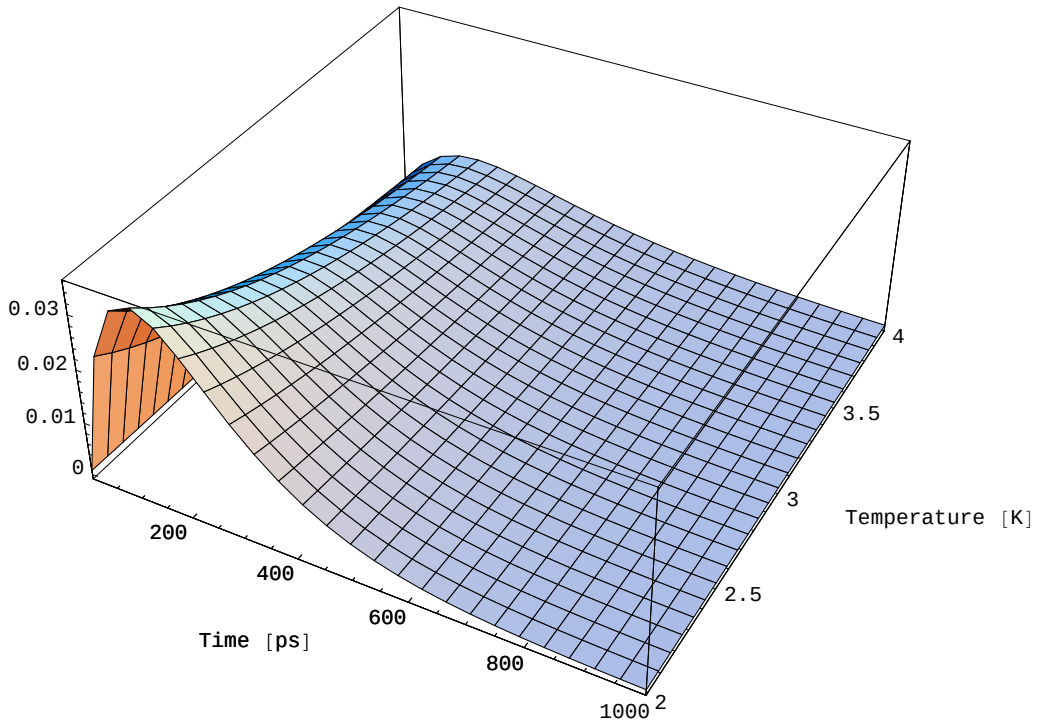

Figure 33: Difference between a signal of a region with equal temperature to a region, where heat diffusion is taken into consideration. The plot shows the difference with a time scale of 1 ps to 1 ns and a temperature scale of 2 to 4 K.

In figure 33 we present the difference of the intensity of the luminescence signal of a region between the situation, where the temperature depends on the position, and the one, where the temperature is equal to that of the bath. The initial intensity of the signal is unity.

On figures 34 and 35 the effect of the intensity of the excitation is reported.

The thermal surface resistance (Kapitza resistance) is know to be proportional to $H = T^3$. For organic materials, there is nothing to be found in the

A Estimation on the Impact of the Thermal Resistance on the Sample Temperature

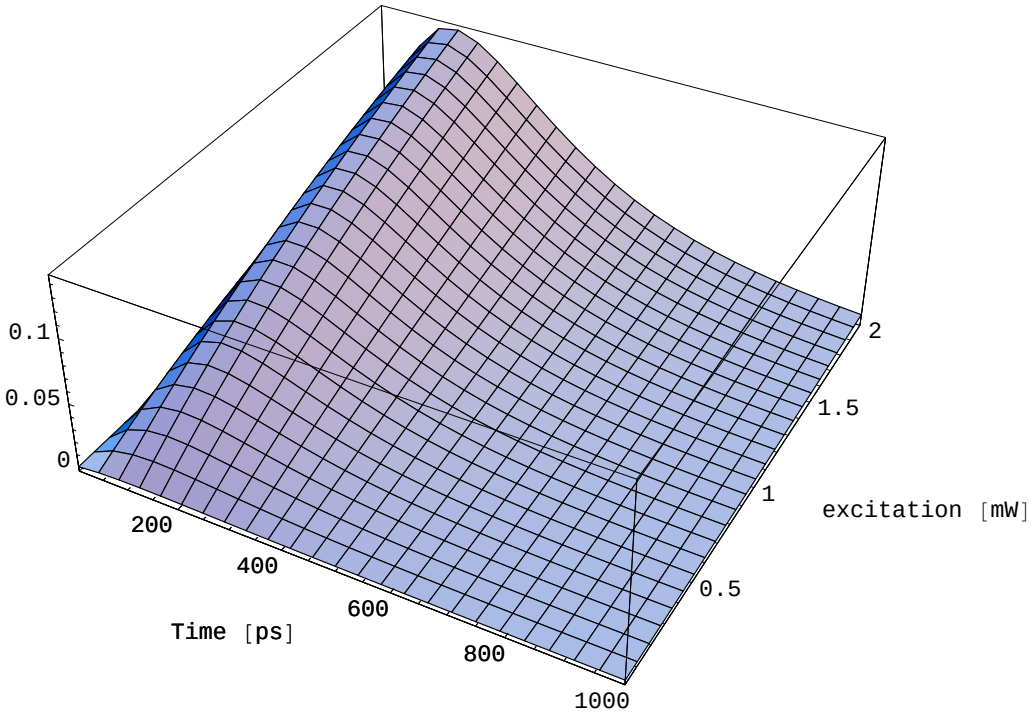

Figure 34: Impact of the excitation intensity at a bath temperature of 2 K. The z axis shows the difference in time to the temporal signal of a region with constant temperature.

A Estimation on the Impact of the Thermal Resistance on the Sample Temperature

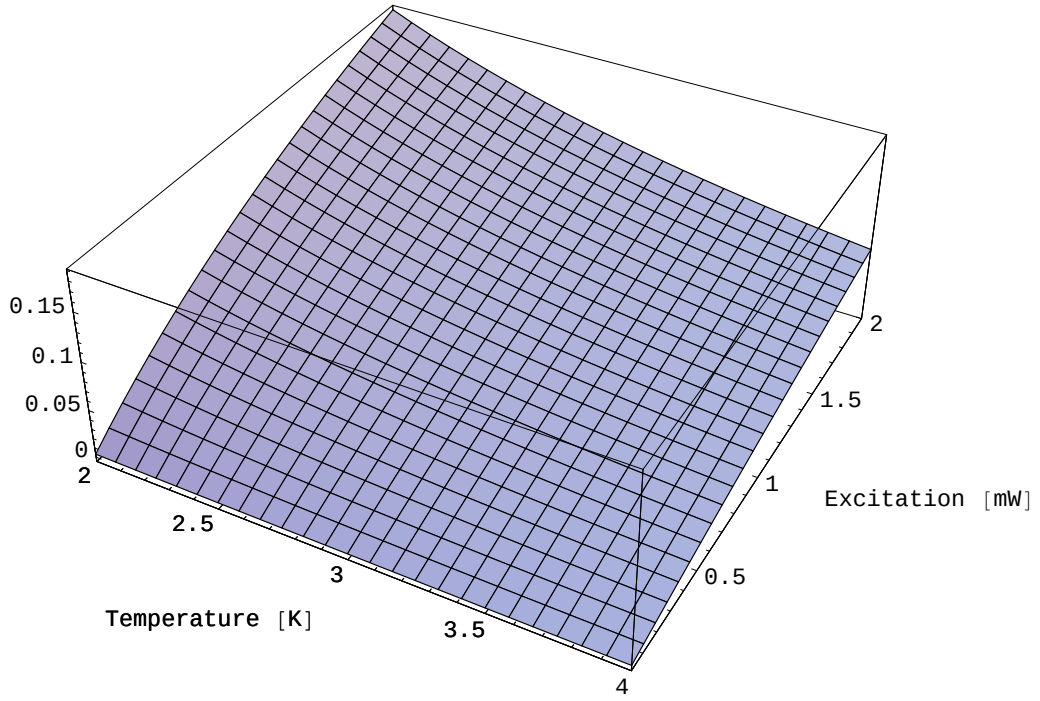

Figure 35: Difference in time at 170 ps in function of the temperature.

literature. One of the best studied interfaces is copper and helium II. [Pol69] gives the following value:

$$R = 0.20 \cdot T^3 \ (cm^2 - ^\circ K/W)$$

The impact of this interface would be a rise in temperature of some 10 mK in the temperature range between 2 and 4 K.

A detailed discussion of the impact of the temperature on the radiative lifetime is placed in chapter 5.4.2.

References

[Abe89] S. Abe. *Exciton versus interband absorption in peierls insulators. Journal of the Physical Society of Japan*, **58**(1):62–65 (1989).

[Aki03] H. Akiyama, M. Yoshita, L. N. Pfeiffer, K. W. West, and A. Pinczuk. *One-dimensional continuum and exciton states in quantum wires. Applied Physics Letters*, **82**(3):379–381 (2003).

[And91] L. C. Andreani, F. Tassone, and F. Bassani. *Radiative lifetime of free-excitons in quantum-wells. Solid State Communications*, **77**(9):641–645 (1991).

[Bae92] D. Baeriswyl, D. Campbell, and S. Mazumdar. *Conjugated conducting polymers*. In H. Kiess, editor, *Springer series in solid state sciences*, volume 102. Springer, Berlin (1992).

[Bared] T. Barisien, L. Legrand, and M. Schott (to be published).

[Bat00] H. Batelaan. *The kapitza-dirac effect. Contemporary Physics*, **41**(6):369–381 (2000).

[Ber04] J. Berréhar, C. Lapersonne-Meyer, M. Schott, and G. Weiser. *A high energy exciton in polydiacetylene chains, involving electrons localized on the triple bond. Chemical Physics*, **303**(1-3):129–136 (2004).

[Bou78] H. Bouchriha, V. Ern, J. L. Fave, C. Guthmann, and M. Schott. *Applicability of kinematic theory to singlet exciton fission in tetracene. Physical Review B*, **18**(1):525–528 (1978).

[Car59] H. Carslaw and J. Jaeger. *Conduction of heat in solids*. Clarendon Press, Oxford, 2nd. edition (1959).

[Cit92] D. S. Citrin. *Long intrinsic radiative lifetimes of excitons in quantum wires. Physical Review Letters*, **69**(23):3393–3396 (1992).

[Cit93] D. S. Citrin. *Radiative lifetimes of excitons in quantum-wells - localization and phase-coherence effects. Physical Review B*, **47**(7):3832–3841 (1993).

[Dub02] F. Dubin, J. Berrehar, R. Grousson, T. Guillet, C. Lapersonne-Meyer, M. Schott, and V. Voliotis. *Optical evidence of a purely one-dimensional exciton density of states*

in a single conjugated polymer chain. *Physical Review B*, **66**(11):– (2002).

[Dub04] F. Dubin. *Exciton dans un fil quantique organique*. Ph.D. thesis, Université Paris VI (2004).

[Eng80] I. Engeln and M. Meissner. *Heat-capacity of a polydiacetylene single-crystal from 3-k to 300-k*. *Journal of Polymer Science Part B-Polymer Physics*, **18**(11):2227–2241 (1980).

[Fit68] D. B. Fitchen. *Physics of color centers*. page 655. Academic Press, New York and London (1968).

[Got97] H. Gotoh, H. Ando, and T. Takagahara. *Radiative recombination lifetime of excitons in thin quantum boxes*. *Journal of Applied Physics*, **81**(4):1785–1789 (1997).

[Haa99] S. Haacke, J. Berrehar, C. Lapersonne-Meyer, and M. Schott. *Dynamics of singlet excitons in 1d conjugated polydiacetylene chains: a femtosecond fluorescence study*. *Chemical Physics Letters*, **308**(5-6):363–368 (1999).

[Hor96] A. Horvath, G. Weiser, C. Lapersonne-Meyer, M. Schott, and S. Spagnoli. *Wannier excitons and franz-keldysh effect of polydiacetylene chains diluted in their single crystal monomer matrix*. *Physical Review B*, **53**(20):13507–13514 (1996).

[Hor97] A. Horvath, G. Weiser, C. LapersonneMeyer, M. Schott, and S. Spagnoli. *Excited pi states in polydiacetylenes: Influence of the chain environment*. *Synthetic Metals*, **84**(1-3):553–554 (1997).

[Kra98] B. Kraabel, M. Joffre, C. Lapersonne-Meyer, and M. Schott. *Singlet exciton relaxation in isolated polydiacetylene chains studied by subpicosecond pump-probe experiments*. *Physical Review B*, **58**(23):15777–15788 (1998).

[Lec98] R. Lecuiller, J. Berrehar, C. Lapersonne-Meyer, and M. Schott. *Dual resonance fluorescence of polydiacetylene chains isolated in their crystalline monomer matrix*. *Physical Review Letters*, **80**(18):4068–4071 (1998).

References

[Lec99] R. Lecuiller, J. Berrehar, C. Lapersonne-Meyer, M. Schott, and J. D. Ganiere. *Fluorescence quantum yield and lifetime of 'red' polydiacetylene chains isolated in their crystalline monomer matrix*. *Chemical Physics Letters*, **314**(3-4):255–260 (1999).

[Lec00] R. Lecuiller. *Chaîne "bleue", chaîne "rouge" : deux structures électroniques des chaînes ordonnées de polydiacétylène*. Ph.D. thesis, Université Paris VI (2000).

[Lec02] R. Lecuiller, J. Berrehar, J. D. Ganiere, C. Lapersonne-Meyer, P. Lavallard, and M. Schott. *Fluorescence yield and lifetime of isolated polydiacetylene chains: Evidence for a one-dimensional exciton band in a conjugated polymer*. *Physical Review B*, **66**(12):125205 (2002).

[Mor86] D. T. Morelli, J. Heremans, M. Sakamoto, and C. Uher. *Anisotropic heat-conduction in diacetylenes*. *Physical Review Letters*, **57**(7):869–872 (1986).

[Obe00] D. Y. Oberli, F. Vouilloz, R. Ambigapathy, B. Deveaud, and E. Kapon. *Photoluminescence study of v-groove quantum wires: The influence of disorder on the optical spectra and the carrier thermalization*. *Physica Status Solidi a-Applied Research*, **178**(1):211–220 (2000).

[Oku98] T. Okuno, H. W. Ren, M. Sugisaki, K. Nishi, S. Sugou, and Y. Masumoto. *Time-resolved luminescence of inp quantum dots in a ga0.5in0.5p matrix: Carrier injection from the matrix*. *Physical Review B*, **57**(3):1386–1389 (1998).

[Pol69] G. L. Pollack. *Kapitza resistance*. *Reviews of Modern Physics*, **41**(1):48 (1969).

[Que93] X. Quelin, B. Perrin, G. Louis, and P. Peretti. *3-dimensional thermal-conductivity-tensor measurement of a polymer crystal by photothermal probe-beam deflection*. *Physical Review B*, **48**(6):3677–3682 (1993).

[Ros96a] F. Rossi and E. Molinari. *Coulomb-induced suppression of band-edge singularities in the optical spectra of realistic quantum-wire structures*. *Physical Review Letters*, **76**(19):3642–3645 (1996).

[Ros96b] F. Rossi and E. Molinari. *Linear and nonlinear optical properties of realistic quantum-wire structures: The dominant role of coulomb correlation.* *Physical Review B*, **53**(24):16462–16473 (1996).

[Sch] M. Schott. *Private communication.*

[Six84] H. Sixl. *Spectroscopy of the intermediate states of the solid-state polymerization reaction in diacetylene crystals.* *Advances in Polymer Science*, **63**:49–90 (1984).

[Spa94] S. Spagnoli, J. Berrehar, C. Lapersonnemeyer, and M. Schott. *Polydiacetylene chains diluted in their single-crystal monomer matrix.* *Journal of Chemical Physics*, **100**(9):6195–6202 (1994).

[Spa95] S. Spagnoli. *Polydiacétylènes cristallins : de la chaine isolée 1D en matrice monomère au film mince de polymère.* Ph.D. thesis, Université Paris VII (1995).

[Spa96] S. Spagnoli, J. Berrehar, C. LapersonneMeyer, M. Schott, A. Rameau, and M. Rawiso. *gamma-ray polymerization of urethane-substituted diacetylenes: Reactivity and chain lengths.* *Macromolecules*, **29**(17):5615–5620 (1996).

[Sun70] A. Suna. *Kinematics of exciton-exciton annihilation in molecular crystals.* *Physical Review B*, **1**(4):1716 (1970).

[Tan89] H. Tanaka, M. A. Gomez, A. E. Tonelli, and M. Thakur. *Thermochromic phase-transition of a polydiacetylene, poly(etcd), studied by high-resolution solid-state c-13 nmr.* *Macromolecules*, **22**(3):1208–1215 (1989).

[Wei92] G. Weiser. *Stark-effect of one-dimensional wannier excitons in polydiacetylene single-crystals.* *Physical Review B*, **45**(24):14076–14085 (1992).

[Wei97] G. Weiser and A. Horvath. *Electroabsorption spectroscopy on p-conjugated polymers.* In N. S. Sariciftci, editor, *Primary photoexcitations in conjugated polymers : molecular exciton versus semiconductor band model.* World Scientific, Singapore (1997).

Curriculum Vitae

Christian Blumer
Rue Neuve 13
1003 Lausanne
christianblumer@bluewin.ch

Birthdate and -place: 17.8.1974 in Brugg (AG)
Swiss nationality with origins in Glarus & Freienstein-Teufen ZH

1994-2001	Studies in physics at the EPFL. Diploma title: *Study of the optical emission of one-dimensional and doped nanostructures in semiconductors using apertured micro-photoluminescence spectroscopy*
summer 1999	Internship at CSEM Zürich: *Characterisation of a SCCD, a BCCD and a new Narrow-channel-BCCD line*
1990-1994	Matura Typus C, Alte Kantonsschule Aarau, Switzerland

Languages

German	mother tongue
French	fluent
English	fluent